Emerging single cell endothelial heterogeneity supports sprouting tumour angiogenesis and growth

Ken Matsumoto[1,2], Florian Rambow[3,4], Fabio Stanchi[1,2], Thomas Mathivet[5], Junbin Qian[6,7], Wolfgang Giese[8], Liqun He[9], Diether Lambrechts[6,7], Bin Zhou[10], Christer Betsholtz[9,11], Jean-Christophe Marine[3,4], Holger Gerhardt[1, 2, 8, 12, 13 *]

[1]Vascular Patterning laboratory, VIB Center for Cancer Biology, Leuven, Belgium

[2]Vascular Patterning laboratory, Department of Oncology, KU Leuven, Leuven, Belgium

[3]Laboratory for Molecular Cancer Biology, VIB Center for Cancer Biology, Leuven, Belgium

[4]Laboratory for Molecular Cancer Biology, Department of Oncology, KU Leuven, Leuven, Belgium

[5]Laboratoire de Neurosciences Expérimentales er Cliniques, Université de Poitiers, INSERM U1084, Poitiers, France

[6]Laboratory of Translational Genetics, VIB Center for Cancer Biology, Leuven, Belgium

[7]Laboratory of Translational Genetics, Center for Human Genetics, KU Leuven, Leuven, Belgium

[8]Integrative Vascular Biology, Max-Delbrück Center for Molecular Medicine, 13125 Berlin, Germany

[9]Department of Immunology, Genetics and Pathology, Rudbeck Laboratory, Uppsala University, Uppsala, Sweden

[10]State key Laboratory of Cell Biology, CAS center for Excellence in Molecular Cell Science, Institute of Biochemistry and Cell Biology, Shanghai Institutes for Biological Sciences, University of Chinese Academy of Sciences, Chinese Academic of Sciences,

26   Shanghai 200031, China.

27   [11]Integrated Cardio Metabolic Centre (ICMC), Karolinska Institute, Huddinge, Sweden

28   [12]DZHK (German Center for Cardiovascular Research) Partner site Berlin

29   [13]Berlin Institute of Health (BIH), Berlin, Germany

30   *Correspondence: H. Gerhardt, email: holger.gerhardt@mdc-berlin.de

31

32   Keywords: *Csf1r*, lineage tracing, tumour angiogenesis, intravital imaging, single cell

33   transcriptional profiling

34   Conflict of Interest: The authors have declared that no conflict of interest exists.

35

36

37   **SUMMARY**

38   Blood vessels supplying tumors are often dysfunctional and generally heterogeneous. The

39   mechanisms underlying this heterogeneity remain poorly understood. Here, using

40   multicolor lineage tracing, *in vivo* time-lapse imaging and single cell RNA sequencing in

41   a mouse glioma model, we identify tumour-specific blood endothelial cells that originate

42   from cells expressing the receptor for colony stimulating factor 1, *Csf1r*, a cytokine which

43   controls macrophage biology. These *Csf1r* lineage endothelial cells (CLECs) form up to

44   10% of the tumour vasculature and express, besides classical blood endothelial cell

45   markers, a gene signature that is distinct from brain endothelium but shares similarities

46   with lymphatic endothelial cell populations. *in silico* analysis of pan-cancer single cell

47   RNAseq datasets highlights the presence of a comparable subpopulation in the

48   endothelium of a wide spectrum of human tumours. We show that CLECs actively

49   contribute to sprouting and remodeling of tumour blood vessels and that selective

50   depletion of CLECs reduces vascular branching and tumour growth. Our findings indicate

51   that a non-tumour resident Csf1r-positive population is recruited to tumours,

52   differentiates into blood endothelial cells to contribute to vascularization and, thereby,

53   tumour growth.

54

55

56   **INTRODUCTION**

57   Endothelial cells form a single cell layer lining the inner walls of blood vessels and play

58   critical roles in organ homeostasis and disease progression. Once formed, following

59   embryonic and early post-natal development, blood vessels retain a high level of

60   adaptability to meet changing metabolic or hemodynamic requirements or enable further

61   tissue growth including in tumours. How local vascular networks respond to these

62   adaptive challenges, rapidly expand, remodel and reestablish homeostasis remains a

63   timely research topic, with many open questions still unresolved. In particular in

64   pathologies, knowledge of the precise nature and origin of new vessel formation,

65   endothelial activation and differentiation steps, and of the mechanisms driving vessel

66   dysmorphia, or preventing effective revascularization in ischemic diabetic complication

67   is critical for new therapeutic approaches. New blood vessel formation in the adult was

68   long believed to arise exclusively by sprouting and proliferation of endothelial cells from

69   local blood vessels without any de novo differentiation from progenitor cells. However,

70   Asahara and coworkers isolated mononuclear cells from human peripheral blood and

71   identified circulating endothelial progenitor cells (EPCs) [1]. These cells were shown to

72   derive from the bone marrow and contribute to endothelial cells in blood vessels in

73   hindlimb ischemia and tumour xenograft mouse model [2,3]. By fluorescent in situ

74   hybridization with sex chromosome-specific probes in patients with cancer after bone

75   marrow transplantation, Peters and coworkers demonstrated that bone marrow-derived

76   stem cells contribute to endothelial cells in human tumour endothelium [4]. The resulting

77   concept of vasculogenesis in the adult raised the prospect of novel therapeutic approaches

78   for ischemic vascular disease and for targeting tumour angiogenesis [5,6]. Interestingly,

79   EPCs also contributed to newly forming lymphatic vessels [7,8]. A vast number of

80   publications since have supported or challenged these initial discoveries, and the

81   occurrence, origin and significance of EPCs continues to be a matter of debate [9-12].

82   Whereas EPCs and other circulating progenitor cells were long thought to origin from the

83   bone marrow, recent studies challenged this idea and suggested the existence of a

84   different yet unknown vascular niche for endothelial progenitor cells that can contribute

85   to blood vessel formation[13].

86

87   **RESULTS**

88   ***A Csf1r cell lineage contributes to blood vascular endothelial cells during glioma***

89   ***growth in mice.***

90   In order to study dynamic macrophage recruitment and blood vessel patterning *in vivo*

91   during glioma growth, we adapted a surgical cranial window model for two-photon

92   microscopy allowing repeated visualization of the same animal over time. We generated

93   spheroids of syngeneic C57BL/6 mouse glioma cells (CT2A or GL261) [14,15] modified to

94   stably express blue fluorescent protein (BFP), and injected them into the mouse cortex,

95   followed by implantation of a glass coverslip [16]. By crossing transgenic *Csf1r (Colony*

96   *stimulating factor 1 receptor)*– specific tamoxifen-inducible Cre driver mice [17] with the

97   *mTmG* Cre reporter mouse line [18], we induced membrane-targeted GFP expression in

98   *Csf1r*-expressing cells and used this stable lineage trace to follow the cell population over

99   time (Fig. 1a, b). As expected, the vast majority of tumour associated macrophages were

100 labelled by GFP in line with their *Csf1r*-dependent recruitment and expansion[19].

4

101   Unexpectedly, however, through the combination of longitudinal live two-photon

102   imaging and lineage tracing, we discovered GFP-positive cells contributing to the tumour

103   vasculature during glioma growth (Fig. 1c). These *Csf1r* lineage endothelial cells

104   (CLECs) frequently emerged at tip cell positions of the growing vasculature, heading

105   blood vessel sprouts in the mouse glioma (Fig. 1d, Supplementary Movie1). Additionally,

106   CLECs were found bridging adjacent capillaries during anastomosis (Fig. 1e).

107   Fluorescent dextran injection confirmed that CLECs contributed to - and were

108   incorporated in the endothelial lining of - functionally perfused blood vessels including

109   lumenized sprouts headed by endothelial tip cells (Fig. 1f). Counterstaining on fixed

110   samples identified that all cells forming blood vessels including the lineage-traced CLECs

111   expressed typical endothelial markers (CDH5, CD31) and lacked macrophage and

112   myeloid cell markers (F4/80, CD45) (Fig. 1g, h, Extended Data Fig. 1). BFP was not

113   expressed in CLECs, demonstrating that they were not derived from glioma cells (Fig.

114   1g).

115   To gain more insight into the nature and significance of CLECs, we isolated and

116   quantified the cell population in the mouse glioma model. By 4 weeks of tumour

117   development (close to the specified humane endpoint of 5 weeks) up to 10% of the tumour

118   vasculature was comprised of cells carrying the *Csfr1* lineage trace. Similar frequencies

119   were found in tumours derived from either of the mouse glioma cell lines, CT2A (Fig. 2a,

120   b), or GL261 (Fig. 2c). Polyclonal antibody staining indicated that *Csf1r* may also be

121   expressed in some brain capillary endothelial cells [20,21]. Recent single cell sequencing of

122   adult mouse brain endothelial cells however did not confirm this notion[22], suggesting that

123   CLECs are unlikely to originate from brain endothelium. Indeed, tamoxifen mediated

124   activation of our transgenic *Csfr1* lineage trace did not label brain endothelial cells in

125   mice lacking tumours, sham operated as well as in the healthy brain parenchyma

126 surrounding implanted tumours (Fig. 2d, e, f). *Csf1r* is important for the embryonic

127 development of microglia and its expression is also detected in adult microglia by single

128 cell RNA sequencing. Surprisingly however, Csf1r-Mer-iCre-Mer mediated

129 recombination of the Cre-Reporter expression was also not observed in microglia of the

130 healthy adult mouse brain. Irrespective of this apparent discrepancy between reported

131 microglial *Csf1r* expression and the lack of Csf1r- Mer-iCre-Mer mediated recombination

132 in microglia, these data also exclude microglia as a potential source of CLECs.

133 Furthermore, we observed CLECs also in tumours originating from B16F1 melanoma

134 cells implanted under the skin; thus, this *Csfr1*-lineage endothelial cell contribution not

135 only occurs in brain tumours with microglia in their environment, but also in other tumour

136 types and locations (Fig. 2g, h). Notably, we also found *Csf1r*-lineage lymphatic

137 endothelial cells in B16F1 skin melanomas indicating that CLECs can contribute to both

138 blood and lymphatic vessels (Extended Data Fig. 2).

139 ***CLECs do not originate from hematopoietic niche in bone-marrow or spleen.***

140 Given the abundant labelling of macrophages and the important role of *Csf1r* in the

141 recruitment of bone-marrow derived monocytes and differentiated macrophages, we

142 asked whether CLECs are also derived from the bone-marrow. To test this possibility, we

143 generated bone marrow chimeras. Flow cytometric analysis confirmed 97.3 ± 1.6 %

144 reconstitution of wild-type recipient bone marrow by transplanted *Csf1r-Mer2.Cre^{mTmG}*

145 bone marrow after 8 weeks post transplantation (Extended Data Fig. 3). Analysis of

146 glioma blood vessels in these bone marrow chimeras (BM^{Csf1r-Mer2.Cre-mTmG}) failed to

147 identify bone marrow derived CLECs, although the numbers of tumour macrophage were

148 similar to controls (Fig. 3a). Conversely, chimeras of wild-type donor bone marrow

149 transplanted into *Csf1r-Mer2.Cre^{mTmG}* recipients (*Csf1r-Mer2.Cre^{mTmG}*::BM^{WT}),

150 displayed similar CLECs numbers in glioma vessels as observed earlier in non-chimeric

151   *Csf1r-Mer2.Cre^mTmG* mice (Fig. 3b). These results were confirmed by intravital imaging

152   in the glioma of *Csf1r-Mer2.Cre^mTmG*::BM^WT (Fig. 3c, Supplemental Movie 2). Thus, the

153   bone marrow chimera and lineage tracing experiments strongly suggest that CLECs do

154   not originate from bone marrow-derived cells, nor do they represent previously suggested

155   transdifferentiation events from bone marrow-derived macrophages. Surgical removal of

156   the spleen also did not affect CLECs numbers, further ruling out spleen-derived

157   macrophages as source of CLECs (Extended Data Fig. 4).

158   ***CLECs regulate vascular patterning and support glioma growth.***

159   In late-stage gliomas, CLECs preferentially localized to the peripheral tumor area,

160   correlating with the zone of most active angiogenesis (Extended Data Fig. 5). Real-time

161   intravital imaging of mouse gliomas also revealed that CLECs incorporation into vessels

162   is very dynamic. This implied that CLECs might have unique and potentially transient

163   functions during tumour vessel formation. To gain a better understanding of CLECs

164   behaviour during tumour growth, we developed dual-recombination combinatorial

165   genetics as a tool for CLECs tracing [23,24]. To achieve selective recombination in CLECs,

166   we used the *Cdh5* endothelial driver for expression of the Dre recombinase, and the same

167   transgenic mouse line as above expressing the tamoxifen inducible form of the Cre

168   recombinase under control of the *Csf1r* transgene. The combined action of these distinct

169   recombinases, Dre and Cre, allowed for deletion of two stop cassettes flanked by RoxP

170   and LoxP sites, respectively, located upstream of a tdTomato expression cassette (Fig.

171   4a). Using this strategy, we could selectively trace tdTomato-positive CLECs in mouse

172   gliomas following tamoxifen exposure (Fig. 4b). Note that the appearance of labelled

173   CLECs and blood vessel labelling differs from the images of the mTmG line, as the dual

174   Dre/Cre tdTomato reporter used lacks a general label of unrecombined cells. Fluorescent

175   dextran injection instead was used to label vascular lumen, highlighting dtTomato

7

176   positive CLECs that line the vessel lumen. As expected, counterstaining on fixed samples

177   demonstrated that CLECs express the prototypical endothelial marker, ERG (ETS-related

178   gene) (Fig. 4c). In order to assess whether CLECs contribute functionally to tumour

179   growth and vascular patterning in glioma, we used the same dual recombination strategy

180   to selectively ablate CLECs (Fig. 4d). In this model, CLECs expressed both GFP as well

181   as the diphtheria toxin receptor after tamoxifen induction enabling depletion of GFP-

182   positive CLECs by administration of diphtheria toxin (Fig. 4e, h). Strikingly, CLECs

183   ablation significantly decreased glioma growth (Fig. 4g, i). CLECs ablation also

184   decreased the vascular network length and the number of bifurcations in tumour vessels

185   (Fig. 4j, k, l), indicating that CLECs may promote tumour growth by supporting vessel

186   branching.

187   ***CLECs express a unique set of markers***

188   To further understand the nature of tumour CLECs (T_CLECs), we performed single-cell

189   RNA sequencing (scRNA-seq) on isolated T_CLECs in the mouse glioma model. Single-

190   cell transcriptome analysis using Smart-seq2 [25] identified that the gene expression pattern

191   of T_CLECs was similar to lineage-negative tumour endothelial cells (T_ECs), but not

192   to tumour macrophages (T_MACs), as determined by UMAP (Uniform Manifold

193   Approximation and Projection) analysis (Fig. 5a). Single-cell differential expression

194   (SCDE) analysis [26] confirmed that T_CLECs expressed typical endothelial markers, but

195   lacked macrophage and myeloid cell markers (Fig. 5b). Unexpectedly, however,

196   T_CLECs showed no *Csf1r* expression, despite carrying the *Csf1r*-lineage marker (Fig.

197   5c). Beyond the overlapping gene expression pattern between T_CLECs and T_ECs,

198   SCDE analysis identified a unique signature that can distinctly define the T_CLECs

199   population; RNAs coding for 24 genes including three types of cell surface proteins

200   (*Aqp1: Aquaporin 1, Fabp4: Fatty acid binding protein 4, Kcnj8: Potassium voltage-*

8

201 *gated channel subfamily j member 8*) were significantly enriched in T_CLECs (Fig. 5d;

202 Extended Data Fig. 6; Supplementary Table 1). *Aqp1* is highly expressed in vascular

203 endothelial cells and was reported to contribute to tumour growth and angiogenesis [27].

204 Staining of lineage traced T_CLECs on fixed mouse glioma samples confirmed AQP1

205 expression (Extended Data Fig. 7).

206 ***The T_CLEC state is enriched for "Tip-like" and a lymphatic gene signature***

207 Gene set enrichment analysis (GSEA) identified that the T_CLEC state shows significant

208 enrichment for a Tip-cell-like associated gene expression program (Fig. 5e), thus

209 supporting the morphological observations and their functional importance for branching

210 and tumour growth. Intriguingly, GSEA identified that T_CLECs were also enriched for

211 lymphatic gene signatures (Fig. 5e). AUCell analysis [28] of scRNA-seq data from multiple

212 human primary tumours identified subpopulations of endothelial cells that express the

213 T_CLECs marker gene set (Fig. 5f-k, 442 out of 7314 ECs are candidates: 6.0%;

214 Supplementary Table 2). These *bona-fide* T_CLECs were highly enriched in tip cell,

215 neophalanx cell, lymphatic endothelial cell subpopulations and particularly abundant in

216 human pancreatic cancer (Fig. 5k). Neophalanx endothelial cells, which express two pro-

217 angiogenesis markers, *Glul (Glutamine synthetase)* and *Cxcl12 (C-X-C motif chemokine*

218 *ligand 12)* [29,30] have recently been identified in lung tumour-associated endothelial cell

219 studies [31,32], and were proposed to line neo-vessels after termination of vessel sprouting.

220 Together this data suggests that based on the transcriptional state, T_CLECs might have

221 a supportive role in tumor vessel sprouting and remodeling. Detailed comparison with

222 recent single cell RNA seq data on tumour endothelial cells in mouse and human tumours

223 [31] confirmed the Tip-like gene signature of T_CLECs, but also identified significant

224 similarities with lymphatics (Fig. 5k). The latter is particularly surprising given that our

9

225 perfusion experiments with dextran clearly demonstrated that T_CLECs in the glioma

226 model line blood vessels, not lymphatics.

227 *Acute recombination identifies a CLEC lineage in lymph nodes*

228 The transcriptional similarities between T_CLECs and lymphatic endothelial cells are

229 noteworthy as blood endothelial cells, in particular in the brain environment, and

230 lymphatic EC represent highly differentiated cell types. During vertebrate embryogenesis,

231 lymphovenous specification sees common progenitor cells diverge in their differentiation

232 to establish mature blood endothelium and lymphatic endothelium[33]. The apparent

233 similarities could therefore suggest that T_CLECs represent an immature endothelial cell

234 state with partially overlapping profiles of both immature blood and lymphatic cells. In

235 this case, the expression of lymphatic genes would signify a return to an earlier cell state

236 or potentially some level of transdifferentiation between the two endothelial cell states.

237 The latter would imply a distant source of lymphatic endothelium as possible origin of

238 CLECs. Indeed, when searching for CLECs in all organs, we observed selective

239 endothelial labelling in lymph nodes, notably restricted to the periphery where specialized

240 lymphatic endothelial cells form the floor of the subcapsular sinus (SCS, Fig. 6a). Bone-

241 marrow transplantation to eliminate the abundant Csfr1-lineage macrophage population

242 highlighted the specific labelling of CLECs in lymph nodes (Fig. 6b).

243 To gain more insight into the emergence of T_CLECs, we asked whether acute

244 recombination could indicate their possible origin. Acute induction experiments (24h

245 after single tamoxifen injection) illustrated that the Csf1r-expressing progenitors of this

246 tumour endothelial cell population do not reside locally in pre-existing brain or the

247 associated brain tumour vasculature (Extended Fig. 8). Close inspection however

248 revealed GFP-positive endothelial cells with significant labelling 24h post-injection in

249 the floor endothelial cells of the SCS of lymph nodes (Fig. 6c). The mTmG Cre-reporter

250   switches from red fluorescent protein expression to mEGFP expression upon

251   recombination. Therefore, cells that acutely recombine, carry both GFP and Tomato

252   expression until the latter is fully degraded. Strikingly, floor SCS endothelial cells

253   exhibited both GFP and simultaneous Tomato expression, demonstrating recent

254   recombination. FACS analysis confirmed the presence of double positive EC in lymph

255   nodes, but not in brain or brain tumours. In fact, double positive cells for GFP and Tomato

256   were not observed in the brain tumours at any stage, excluding the possibility of any acute

257   or continuous local recombination of T_CLECs within the tumour microenvironment.

258   Prox-1 staining confirmed the lymphatic nature of CLECs in the lymphnode, and

259   demonstrated that only a subpopulation of lymphatic endothelial cells in the lymph node

260   carry the Csfr1-lineage trace, the cells in the floor of the SCS (Fig. 6d).

261   We decided to perform scRNA seq also on endothelial cells isolated from lymph nodes,

262   assess gene expression and perform pseudotime analysis to understand differentiation of

263   T_CLECs, T_EC, LN_CLECs (GFP positive) and LN_ECs (GFP negative) (Fig. 7a-f).

264   We used the same Smart-seq2 platform for comparison to sequence another 384 cells of

265   lymph node origin. After quality control (Fig. 7a), 89 cells EC, not Csfr1 lineage EC, and

266   104 cells expressing GFP (Fig.7b) in the lymph nodes were selected for further analysis.

267   Comparative analysis with recent mouse lymph node scRNA data[34] confirmed that the

268   LN_CLEC co-register with identified SCS floor cells (Extended Data Fig. 9a).

269   Unlike T_CLECs, LN_CLECs also expressed Csf1r, in line with our finding of acute

270   recombination in the SCS floor cells.

271   UMAP based dimension reduction placed T_CLECs and T_EC closely together, as before,

272   and also LN_CLEC and LN_EC co-cluster, although two additional distinct LN_EC

273   clusters appear highly distinct and thus unrelated to any of the other cell types (Fig. 7c).

274   Interestingly, some T_CLEC cluster with the LN_CLEC, suggesting that there is at least

275   some overlap in gene expression between the Csf1r lineage cells in the brain tumour and

276   in the lymph nodes. Looking at relative expression levels of all genes in a heatmap

277   comparing the lineage positive and negative EC from lymph nodes and tumours

278   highlighted that differential expression is more prevalent than any overlap between

279   tumour EC and LN EC (Fig. 7d). However, there are small number of genes like Pde4d,

280   Robo1 and Itga9 that show higher expression in the two lineage positive populations in

281   LN and tumour, compared to the lineage negative cells (Extended Data Fig. 9b). Itga9 is

282   well known to be important in lymphatic development[35], confirming again that T_CLECs

283   carry some gene expression patterns normally associated with lymphatic EC.

284   Nevertheless, despite the fact that only LN_CLEC appear to acutely recombine,

285   differential gene expression analysis does not provide clear evidence for a lineage

286   relationship between LN_CLEC and T_CLEC.

287

288   ***T_EC and T_CLECs "co-evolve" during tumour growth, suggesting distinct origin***

289   To gain more insight into the differentiation state and possible route of differentiation,

290   we next performed pseudotemporal ordering using Monocle[36] (Fig. 7f). The Monocle

291   inferred trajectory suggested equally distributed pseudotime values for T_CLECs and

292   T_EC then LN_EC and finally LN_CLECs. When measuring single-cell gene expression

293   diversity as surrogate for differentiation potential with the CytoTRACE algorithm[37]

294   (higher score means more undifferentiated, stem-like), we observed again equal scores

295   between T_CLECs and T_EC but lower cytoTRACE values for LN_EC and LN_CLECs

296   (Fig. 7e-f). The equal scores between T_CLECs and T_ECs argue against a role of T_ECs

297   as precursors for T_CLECs, independently confirming that T_CLECs are unlikely

298   emerging through differentiation from the pre-existing brain tumour vasculature.

299   However, the LN_CLECs display the lowest cytoTRACE scores (most differentiated).

300   Based on the cytoTRACE analysis, and its logic of developmental potential, it would

301   seem unlikely that LN_CLEC are the origin of T_CLEC (Fig. 7e-f). Moreover, it appears

302   that both lineage positive and negative EC in the lymph nodes are more differentiated

303   than endothelial cells in the tumour. It is noteworthy that Monocle was designed for

304   developmental questions, which are strictly unidirectional. Interestingly, when plotting

305   CytoTRACE scores onto the Monocle trajectory (Fig. 7f), the right side shows higher

306   scores (T_CLEC and T_EC) and the left side (darker blue) lower scores (LN_CLECs

307   lowest), being in line with pseudotime. This again predicts that LN_CLECs represent an

308   end state rather than the origin. In summary, these data predict that during tumour growth,

309   the T_EC and T_CLECs coevolve from a distinct origin to then share many aspects of

310   their gene expression and biology, yet with a few very distinct gene profiles.

311

312   **DISCUSSION**

313   In this study, using inducible *Csf1r* lineage tracing in adult mice intended to study

314   macrophage recruitment during glioma development, we identify a distinct endothelial

315   cell lineage that forms up to 10% of the tumour vasculature in adult mice. Selective

316   experimental depletion of this *Csf1r* endothelial cell lineage demonstrated a role in

317   promoting vascular branching and tumour growth. Through a combination of genetic

318   lineage tracing, longitudinal live two-photon imaging, and single cell analysis, we find

319   that these cells arise during tumour progression, adopt dynamic endothelial phenotypes

320   including tip cell characteristics, and express common endothelial as well as unique

321   markers that can also be found in patient-derived tumour endothelium.

322   *Csf1r* is a well-known regulator of monocyte/ macrophage differentiation [38,39], but is

323   also important for yolk sac hematopoiesis and progenitor cell differentiation. Klotz and

324   coworkers reported that *Csf1r*-expressing cells in the mouse embryo contribute to *Prox1-*

325   positive lymphatic endothelial cells in the cardiac lymphatic vasculature [40]. Moreover, a

326   recent report identified that *Csf1r*-expressing erythro-myeloid progenitors from the early

327   embryonic yolk-sac could give rise to intraembryonic endothelial cells in mouse

328   development[41]. *Csf1r* is also expressed in EPCs, such as colony forming unit-Hill cells

329   and circulating angiogenic cells [42]. In the adult however, *Csf1r* is not expressed in the

330   mature endothelium of blood and lymphatic vessels, but continues to drive recruitment

331   and expansion of myeloid cells in inflammation, ischemia and tumour growth [43].

332   Intriguingly, *Csf1r* itself is no longer expressed in the Csf1r lineage cells within the

333   tumour and acute recombination of endothelial cells 24h after tamoxifen injection fails to

334   label cells in the tumour vasculature. These results raise the possibility that a *Csf1r-*

335   *expressing cell population* of endothelial nature or potential is present elsewhere in the

336   body, recombines upon tamoxifen injection and is recruited to the tumour vasculature

337   where it differentiates into blood endothelium to contribute to tumour angiogenesis.

338   Alternatively, the fact that Csf1r expression is not detected in isolated tumour CLECs

339   could also indicate that the Cre-line is leaky and gives rise to labelled cells through

340   stochastic recombination. In that case, one would expect the labelled cells to populate any

341   part of the vasculature and be otherwise indistinguishable from the unlabelled tumour EC.

342   Single cell analysis however identifies a unique gene expression signature beyond the

343   large number of genes that are co-expressed in T_CLEC and T_EC, and demonstrates

344   that T_CLEC are distinctly enriched in tip-cell and neo-phalanx cell populations. Thus,

345   labelled cells show distinct phenotypes, location and expression patterns, ruling out

346   purely stochastic recombination events. Furthermore, such stochastic recombination

347   within the tumour vasculature would necessitate that we identify acutely labelled cells

348   marked by co-expression of Tomato and GFP. As we failed to identify such cells at any

349   timepoint during tumour growth, and also could detect the emergence of T_CLECs in

14

350   mice only injected with tamoxifen before tumour implantation, the cumulative evidence

351   would suggest that T_CLECs originate outside of the tumour and also that the progenitor

352   population resides outside of the brain. Despite all our efforts, the present work fails to

353   provide ultimate and definitive proof of the true origin of T_CLECs, but arrives at a clear

354   direction and working hypothesis for future studies. In search of their origin and a

355   potential progenitor population, we imaged and analysed all organs by FACS. We

356   performed bone-marrow transplantation, performed splenectomy and examined the entire

357   mouse by fluorescence stereomicroscopy after clearing to identify regions of

358   recombination. The results of bone-marrow transplantation effectively ruled out EPC or

359   any other known progenitors that may be found in circulation, including

360   transdifferentation from macrophages. Four independent observations placed a spotlight

361   on lymphatics, and the lymph nodes in particular. First, the only *bonafide* Csf1r lineage

362   endothelial cell population that we could identify outside of the tumours, including after

363   complete reconstitution of the bone marrow by wildtype bone marrow, was found in the

364   subcapsular sinus of the lymph nodes. Here the floor cells, specialized lymphatic

365   endothelial cells that we identify as GFP and Csf1r positive line the capsule in lymph

366   nodes in close apposition to the Csf1 expressing ceiling cells. Second, after acute

367   tamoxifen injection the cells in the floor of the subcapsular sinus are uniquely double

368   positive for Tomato and GFP, demonstrating acute and likely local recombination. Third,

369   single cell RNAseq of T-CLECs identified lymphatic markers including the lymphatic

370   master regulator Prox1 co-expressed with blood endothelial markers, and SCDE placed

371   T_CLECs close to lymphatic endothelial cells from various mouse tumour models in

372   recently published datasets. And finally, CLECs can also be found in lymphatics in

373   subcutaneous tumour models and in skin. These independent observations clearly make

374 the SCS floor cells prime candidates for the origin of T_CLECs, but future work will be

375 necessary for a possible direct demonstration of this link.

376 In developmental studies, lineage relationships have recently been studied by scRNAseq

377 data sets through pseudotime analysis. In particular the CytoTRACE analysis can be

378 useful to estimate the degree of differentiation of cell populations and thereby also predict

379 their stemness [37]. Our comparative analysis of endothelial cells isolated from tumour and

380 lymph nodes assigned the highest differentiation scores to cells in the lymph node, and

381 lower values to the EC in tumour, including T_CLECs. Accordingly, the cells in the floor

382 of the SCS that carry the lineage label would rather be assumed at the end of a

383 differentiation process rather than progenitors for other populations such as the T_CLECs.

384 Whether however such algorithms are suitable to determine the potential of endothelial

385 cells to become activated and possibly transdifferentiate is unclear. In particular given the

386 altered environmental context of EC within a growing tumour compared to a vascular bed

387 in homeostasis. The combined monocle[36] and cytoTRACE analysis would fit with a

388 general level of dedifferentiation of endothelial cells within the tumour microenvironment,

389 and therefore a co-evolution of the cell states of both T_EC and T_CLEC. It is likely that

390 pseudotemporal ordering of endothelial cells in a reactivation state will always show the

391 reactivated cells, like in the tumour environment as less differentiated. Indeed, recent

392 work studying the effect of chronic hypoxia on brain endothelium illustrated the wide

393 range of reactivation, in particular noting a strong increase in tip cell population amongst

394 the brain endothelial cells[44]. The current assumption states that these new tip cells arise

395 under hypoxia from pre-existing brain endothelial cells, and possibly emerge from

396 particular endothelial subpopulations. In the absence of lineage tracing, an alternative

397 possibility, raised by our current observation in tumour angiogenesis, could be that new

398 tip cells arise at least in part elsewhere, and are recruited to the hypoxic vessel areas.

399   More work on vascular single cell analysis will be required to establish the fundamental

400   principles of endothelial activation and their interpretation for the different tissue

401   challenges that require vascular adaptations.

402   Angiogenesis is essential for tumour growth, and contributes to metastasis [45,46]. Early

403   hopes that targeting tumour angiogenesis may prove uniquely selective and effective as

404   anti-tumour treatment have, however, been disappointing. Intense research efforts

405   therefore currently focus on understanding reasons and mechanisms for resistance to anti-

406   angiogenic therapy, and identifying new cellular and molecular targets to effectively

407   modify the tumour vasculature [47]. Intravital imaging shows that T_CLECs arise during

408   tumour progression, adopt endothelial phenotypes with tip cell characteristics and line

409   perfused vascular tubes. Consistent with this observation, AUCell analysis of scRNA-seq

410   data in human samples identifies that T_CLECs signatures are highly enriched in tip cell

411   subpopulation. A recent study using single-cell transcriptome analysis revealed that anti-

412   VEGF (vascular endothelial growth factor) treatment reduces the proportion of

413   endothelial tip-like cells in a tumour xenografts [48]. How CLECs affect the outcome of

414   anti-angiogenic treatment will be important to investigate in the future. Considering that

415   T_CLECs prominently express *Vegfr3*, even more so than regular endothelial cells in the

416   tumour, we can speculate that T_CLECs are resistant to anti-VEGFR2 treatment, and

417   possibly escape treatment through the activity of VEGFR3. If so CLECs may adversely

418   affect anti-angiogenic therapy targeting VEGFR2 selectively. Tumour blood vessels are

419   generally highly tortuous and the branching pattern is greatly different from normal blood

420   vessels. Our results from the selective targeting of CLECs in the mouse glioma model

421   show that CLECs ablation decreases both vessel branching and tumour growth. Thus, in

422   the absence of CLEC, the dysmorphic vascular phenotype in tumours appears exacerbated,

423   suggesting that CLECs support the formation of a highly branched vascular network,

17

424   which in turn better promotes tumour growth. Future work will be required to identify the

425   true origin of T_CLECs and to extend this functional analysis to fully appreciate the

426   consequence and opportunities to target or utilize CLECs for therapeutic approaches.

427

428

429   **METHODS**

430   *Mice*

431   Mice expressing both the *Csf1r-Mer-iCre-Mer* transgene (*Csf1r-Mer2.Cre*) [17] and the

432   *Rosa^mTmG* Cre recombination reporter [18] were generated by breeding. Mice carrying the.

433   Endothelial specific *Cdh5-Dre* mice [24] were mated with *Csf1r-Mer2.Cre* mice and

434   *Rosa26-RSR-LSL-tdTomato* mice [23] to obtain *Cdh5-Dre*:: *Csf1r-Mer2.Cre*:: *Rosa26-RSR-*

435   *LSL-tdTomato* mice (*DreMer2.Cre^tdTomato*) that allows combinatorial genetics as a tool for

436   CLECs tracing.   Endothelial specific *Cdh5-Dre* mice were mated with *Csf1r-Mer2.Cre*

437   mice and *Rosa26-RSR-mTmG-DTR* mice to obtain *Cdh5-Dre*:: *Csf1r-Mer2.Cre*:: *Rosa26-*

438   *RSR-mTmG-DTR* mice (*DreMer2.Cre^mTmG-DTR*) that allows for selective tracing and

439   ablation of CLECs. *Rosa26-RSR-mTmG-DTR* mice were designed by Dr. Fabio Stanchi

440   and generated by the team of Dr. Ralf Kühn at the Max Delbrück Center in Germany. All

441   mouse strains were maintained on C57BL/6J background. Animal housing and all

442   experimental procedures were approved by the Institutional Animal Care and Research

443   Advisory Committee of the KU Leuven (085/2016).

444   *Cell lines*

445   CT2A, GL261 glioma cell lines and B16F1 melanoma cell line were cultured in DMEM

446   (Life Technologies) supplemented with 10% FBS (Life Technologies), 1% penicillin/

447   streptomycin (Life Technologies) and 1% glutamine (Life Technologies). Spheroids were

448   obtained by seeding the glioma cells for 48h on non-adherent culture dishes. Spheroids

18

449   of 200- 250μm were selected for implantation.

450   ***Intravital imaging on mouse gliomas***

451   Surgery for tumor implantation, installation of cranial windows and *in vivo* imaging were

452   performed as described previously [16]. Briefly, 8– 12-weeks-old mice were anesthetized

453   with ketamine/ xylazine and a craniotomy was performed on the parietal bone. Spheroids

454   of CT2A or GL261 cells modified to express the blue fluorescent protein TagBFP [50] were

455   injected in the exposed parietal brain cortex, which was then sealed by cementing a glass

456   coverslip to the bone surrounding the craniotomy. After surgery, mice were injected

457   intraperitoneally with tamoxifen (65 μg/g body weight) every 5 days. For CLECs

458   depletion, mice were injected intraperitoneally with diphtheria toxin (4 ng/g body weight)

459   the next day after tamoxifen induction. Longitudinal *in vivo* imaging of growing tumors

460   was performed in mice under isoflurane anesthesia using a SP8 upright microscope (Leica

461   Microsystems) equipped with a HCX IRAPO L25x/0.95 water objective and a Titanium:

462   Sapphire laser (Vision II, Coherent Inc.) tuned at 925 nm. Humane end-point of

463   experiments was applied if animals lost 15-20% of their original weight or shown evident

464   signs of distress.

465   ***Immunofluorescence imaging***

466   Mice anesthetized with ketamine/ xylazine were perfused through the heart with 15 ml of

467   ice-cold PBS, followed by 10 ml of 2% PFA in PBS. Tumour tissues or organs were

468   harvested and fixed overnight in 4% PFA. For tumour tissues, sections (200 μm-thick)

469   were prepared with a vibratome 650V (Thermo Scientific). For organ samples, frozen

470   sections (10 μm-thick) were prepared with a cryostat NX70 (Thermo Scientific). For

471   immunofluorescence imaging studies, the PFA-fixed sections were blocked and

472   permeabilized in TNBT (0.1 M Tris, pH 7.4, 150 mM NaCl, 0.5% blocking reagent from

473   Perkin Elmer, 0.5% Triton X-100) for 4h at room temperature. Sections were incubated

19

474   with antibodies against CDH5 (1:25, AF1002, R&D), CD31 (1:100, ab28364, Abcam),

475   F4/80 (1:100, MF48000, Invitrogen), CD45 (1:100, 550539, BD Pharmingen),   CD169

476   (1:100, 142401, Biolegend), PROX1 (1:200, 11-002, Angiobio), AQP1 (1:4000, AB2219,

477   Millipore), LYVE1 (1:100, 50-0433-80, eBioscience) diluted in TNBT buffer overnight

478   at 4°C, washed in TNT buffer (0.1 M Tris pH 7.4; 150 mM NaCl, 0.5% Triton X-100)

479   and incubated with an Alexa Fluor conjugated antibodies (1:200, ThermoFisher

480   Scientific). Sections were washed and mounted in fluorescent mounting medium (Dako).

481   Images were obtained with a Leica TCS SP8 confocal microscope.

482   *Flow cytometric analysis*

483   Mice were anesthetized with ketamine/ xylazine, then tumour tissues or organs were

484   harvested and incubated with PBS containing 1mg/ml collagenase I (Gibco), 2 mg/ ml

485   Dispase I (Gibco), 100ug/ml DNase I (Roche) and 2 mM $CaCl_2$ for 30 min at 37 °C. After

486   incubation, the digested tissue was passed through a cell strainer and then washed by PBS

487   including 2% FBS. For red cell exclusion, we incubated samples with red cell lysis buffer

488   (Sigma) for 5 min at 37 °C and then washed by PBS including 2% FBS and 2 mM EDTA.

489   Cells were stained with the following monoclonal antibodies: PE/ Cy7 anti-CD45

490   (552848, BD), APC anti-CD31 (561814, BD). Data acquisition was performed with BD

491   FACSVerse and analysis was performed with BD FACSuite software, and FlowJo

492   software.

493   *Mouse melanoma model*

494   Mice (8–12-weeks-old) were anesthetized with ketamine/ xylazine and then 1×10^6 B16F1

495   melanoma cells in PBS were implanted into the right flank region of the mice. B16F1

496   melanomas were removed from mice 12 days after implantation for immunofluorescent

497   imaging studies and flow cytometric analysis. Mice were injected intraperitoneally with

498   tamoxifen (65 µg/g body weight) 4 time/ 2 weeks before tumour implantation and then

20

499   intraperitoneally with tamoxifen (65 µg/g body weight) every 5 days after tumour

500   implantation.

501   ***Single cell isolation and RNA-sequencing***

502   Single cells were sorted (BD FACSAriaIII) in 96 well plates (VWR) containing 2 µL of

503   PBS including 0.2% Triton X-100 and 4U of RNase inhibitor (Takara) per well. Plates

504   were properly sealed and spun down at 2000 g for 1 min before storing at −80°C. Whole

505   transcriptome amplification was performed with a modified SMART-seq2 protocol as

506   described previously [25], using 20 instead of 18 cycles of cDNA amplification. PCR

507   purification was realized with a 0.8:1 ratio (ampureXP beads:DNA). Amplified cDNA

508   quality was monitored with a high sensitivity DNA chip (Agilent) using the Bioanalyzer

509   (Agilent). Sequencing libraries were performed using the Nextera XT kit (Illumina) as

510   described previously [25], using 1/4th of the recommended reagent volumes and 1/5th of

511   input DNA with a tagmentation time of 9 min. Library quality was monitored with a high

512   sensitivity DNA chip (Agilent) using the Bioanalyzer (Agilent). Indexing was performed

513   with the Nextera XT index Kit V2 (A-D). Up to 4 x 96 single cells were pooled per

514   sequencing lane. Samples were sequenced on the Illumina NextSeq 500 platform using

515   75bp single-end reads.

516   ***scRNA-sequencing data analysis***

517   BAM files were converted to merged, demultiplexed FASTQ files, cleaned using fastq-

518   mcf (ea-utils r819), and QC checked with FastQC (0.11.4). Reads were then mapped to

519   the mouse genome (mm18) using STAR (2.4.1b) and quantified with Subread (1.4.6-p2).

520   Cells with less than 100,000 reads and/or 500 genes expressed, more than 20%

521   mitochondrial reads, and less than an average expression level of 3.0 of about 80

522   housekeeping genes [51] were discarded. 469 cells passed these stringent quality criteria.

523   Winsorized Highly Variable genes (HVGs) were identified for tumor derived

21

524 macrophages (T_MACs), endothelial cell (T_ECs) and *Csf1r* lineage endothelial cells

525 (T_CLECs) [26]. These cells were then clustered based on HVG expression using non-

526 negative matrix factorization as dimension reduction approach (run=40, rank=10, in MeV

527 4.8.1). The "best fit" (numbers of clusters) was chosen based on the highest cophenetic

528 correlation coefficient. Next, Single-cell Differential Expression analysis (SCDE) was

529 performed between the different NMF-clusters using the global gene expression matrix

530 [26]. Expression values were library-size-factor-normalized (DESeq) and log2 transformed

531 (log2+1). T_MAC, T_EC, T_CLEC and LN_CLECS, LN_EC, T_CLEC, T_EC cells

532 were projected into a two-dimensional space using Uniform Manifold Approximation and

533 Projection (dims=15, resolution = 0.4) based on 5k most variable features (Seurat

534 pipeline) [52]. Monocle (2.14) based trajectory analysis was performed on T_CLEC, T_EC,

535 LN_CELC and LN_EC (total=454 cells) taking into account n=790 m3Drop genes. The

536 same data set was subjected to CytoTRACE analysis using the online tool

537 (https://cytotrace.stanford.edu/) [37].

538

539 ***AUCell analysis of human scRNA-seq data in multiple tumours***

540 The droplet-based scRNA-seq data of 4 human tumour types were downloaded from

541 publicly available sources including lung cancer (ArrayExpress: E-MTAB-6149 and E-

542 MTAB-6653)[53], PDAC (GSA: CRA001160)[54], liver cancer (GEO: GSE125449)[55], and

543 BCC (GEO: GSE123814)[56]. These datasets were processed and clustered per tumour type

544 using Seurat (v3.0.4) package, and the endothelial cell clusters were identified using

545 marker genes (*CLDN5*, *VWF*, *PECAM1*). The resulting endothelial cell data were pooled

546 together and aligned using anchor-based canonical correlation analysis (CCA) to mitigate

547 the difference related to distinct tumor types and scRNA-seq technologies. Initial graph-

548 based clustering identified 10 clusters including 3 potential doublet clusters as predicted

549   by DoubleFinder (v2), which were subsequently removed before second round of

550   clustering. The resulting 8 clusters consisting of 7314 endothelial cells were annotated

551   based on known marker genes, and their CLECs signature were calculated using AUCell

552   package (v1.6.1). The threshold of AUC score was chosen at the peak of the right modal,

553   and the percentage of putative CLECs were calculated for different subtypes and their

554   tumour type of origin.

555   ***Generation of bone marrow chimeras***

556   Recipient 8-10-weeks-old mice were lethally irradiated (9.5 Gy) and then intravenously

557   injected with $1x10^7$ bone marrow cells from donor mice 16 h later. Tumour implantation

558   experiments were initiated 8 weeks after bone marrow reconstitution. Reconstitution rate

559   was determined using flow cytometric analysis in the peripheral blood.

560   ***Surgical removal of the spleen***

561   Mice (8–12-weeks-old) were anesthetized with ketamine/ xylazine and then the spleen

562   was gently taken out from the connective tissue, while cauterizing associated vessels. The

563   incision was thereafter sutured. These procedures were performed as described previously

564   [57].

565   ***Vessel morphology analysis***

566   Confocal images of the tumour vasculature were analyzed for two-dimensional vessel

567   area, network length and number of network bifurcation points. The tdTomato and GFP

568   channels were merged and a Gaussian blur filter as well as Otsu thresholding was applied

569   to obtain binary vessel mask for sectional area estimation. To obtain the vessel network,

570   a semi-automatic multicut workflow from ilastik [58] was applied to all images. The

571   segmented vessels were skeletonized and converted into a network graph with nodes and

572   edges by using the Python package ImagePy [59]. The lengths of network edges were

573   summed up to obtain the total network length for each image, all nodes with a degree of

574 three or more were counted as bifurcations.

575 *Statistics*

576 Statistical analyses of data were performed with GraphPad Prism 7.0 software. All data

577 are shown as the means ± standard deviations. Differences were assessed using a two-

578 tailed unpaired Mann-Whitney's U test or two-tailed unpaired Welch's correction.

579

580 **AUTHOR CONTRIBUTIONS**

581 KM led and conceived the project, designed and performed experiments, analysed and

582 interpreted data. FR, FS, TM, WG, LH, JQ performed experiments and analyzed data.

583 DL, BZ, CB, JM and HG analyzed data. HG conceived and supervised the project. KM

584 and HG wrote and edited the manuscript, with contribution by all authors.

585

586 **ACKNOWLEDGEMENT**

597

598 **CODE AVAILABILITY**

599   The computational code (R) used for scRNA-seq analysis is based on already published

600   pipelines (see Material and Methods) and available upon request.

601

602   **DATA AVAILABILITY**

603   All scRNA-seq data are available at Gene Expression Omnibus under accession number

604   GSE157507.

605

606   **STATISTICS**

607   Differences were assessed using either a two-tailed unpaired Mann-Whitney's or two-

608   tailed unpaired t-test with Welch correction. All planned comparisons were considered

609   stand-alone and were not corrected for multiple testing.

610

611   **REFERENCES**

612   1   Asahara, T. *et al.* Isolation of putative progenitor endothelial cells for

613   angiogenesis. *Science* **275**, 964-967, doi:10.1126/science.275.5302.964 (1997).

614   2   Shi, Q. *et al.* Evidence for circulating bone marrow-derived endothelial cells.

615   *Blood* **92**, 362-367 (1998).

616   3   Asahara, T. *et al.* Bone marrow origin of endothelial progenitor cells responsible

617   for postnatal vasculogenesis in physiological and pathological neovascularization.

618   *Circ Res* **85**, 221-228, doi:10.1161/01.res.85.3.221 (1999).

619   4   Peters, B. A. *et al.* Contribution of bone marrow-derived endothelial cells to

620   human tumor vasculature. *Nat Med* **11**, 261-262, doi:10.1038/nm1200 (2005).

621   5   Rafii, S., Lyden, D., Benezra, R., Hattori, K. & Heissig, B. Vascular and

622   haematopoietic stem cells: novel targets for anti-angiogenesis therapy? *Nat Rev*

623   *Cancer* **2**, 826-835, doi:10.1038/nrc925 (2002).

25

624   6   Rafii, S. & Lyden, D. Therapeutic stem and progenitor cell transplantation for

625   organ   vascularization   and   regeneration.   *Nat   Med*   **9**,   702-712,

626   doi:10.1038/nm0603-702 (2003).

627   7   Religa, P. *et al.* Presence of bone marrow-derived circulating progenitor

628   endothelial cells in the newly formed lymphatic vessels. *Blood* **106**, 4184-4190,

629   doi:10.1182/blood-2005-01-0226 (2005).

630   8   Kerjaschki, D. *et al.* Lymphatic endothelial progenitor cells contribute to de novo

631   lymphangiogenesis   in   human   renal   transplants.   *Nat   Med*   **12**,   230-234,

632   doi:10.1038/nm1340 (2006).

633   9   Purhonen, S. *et al.* Bone marrow-derived circulating endothelial precursors do not

634   contribute to vascular endothelium and are not needed for tumor growth. *Proc*

635   *Natl Acad Sci U S A* **105**, 6620-6625, doi:10.1073/pnas.0710516105 (2008).

636   10   Kerbel, R. S. *et al.* Endothelial progenitor cells are cellular hubs essential for

637   neoangiogenesis of certain aggressive adenocarcinomas and metastatic transition

638   but not adenomas. *Proc Natl Acad Sci U S A* **105**, E54; author reply E55,

639   doi:10.1073/pnas.0804876105 (2008).

640   11   Basile, D. P. & Yoder, M. C. Circulating and tissue resident endothelial progenitor

641   cells. *J Cell Physiol* **229**, 10-16, doi:10.1002/jcp.24423 (2014).

642   12   Psaltis, P. J. & Simari, R. D. Vascular wall progenitor cells in health and disease.

643   *Circ Res* **116**, 1392-1412, doi:10.1161/CIRCRESAHA.116.305368 (2015).

644   13   Fujisawa, T. *et al.* Endothelial Progenitor Cells Do Not Originate From the Bone

645   Marrow.   *Circulation*   **140**,   1524-1526,

646   doi:10.1161/CIRCULATIONAHA.119.042351 (2019).

647   14   Martinez-Murillo, R. & Martinez, A. Standardization of an orthotopic mouse

648   brain tumor model following transplantation of CT-2A astrocytoma cells. *Histol*

649   *Histopathol* **22**, 1309-1326, doi:10.14670/HH-22.1309 (2007).

650 15 Zagzag, D. *et al.* Expression of hypoxia-inducible factor 1alpha in brain tumors:

651   association with angiogenesis, invasion, and progression. *Cancer* **88**, 2606-2618

652   (2000).

653 16 Stanchi, F., Matsumoto, K. & Gerhardt, H. Imaging Glioma Progression by

654   Intravital Microscopy. *Methods Mol Biol* **1862**, 227-243, doi:10.1007/978-1-

655   4939-8769-6_16 (2019).

656 17 Qian, B. Z. *et al.* CCL2 recruits inflammatory monocytes to facilitate breast-

657   tumour metastasis. *Nature* **475**, 222-225, doi:10.1038/nature10138 (2011).

658 18 Muzumdar, M. D., Tasic, B., Miyamichi, K., Li, L. & Luo, L. A global double-

659   fluorescent Cre reporter mouse. *Genesis* **45**, 593-605, doi:10.1002/dvg.20335

660   (2007).

661 19 Mathivet, T. *et al.* Dynamic stroma reorganization drives blood vessel dysmorphia

662   during glioma growth. *EMBO Mol Med* **9**, 1629-1645,

663   doi:10.15252/emmm.201607445 (2017).

664 20 Raivich, G. *et al.* Regulation of MCSF receptors on microglia in the normal and

665   injured mouse central nervous system: a quantitative immunofluorescence study

666   using confocal laser microscopy. *J Comp Neurol* **395**, 342-358,

667   doi:10.1002/(sici)1096-9861(19980808)395:3<342::aid-cne6>3.0.co;2-2 (1998).

668 21 Jin, S. *et al.* Interleukin-34 restores blood-brain barrier integrity by upregulating

669   tight junction proteins in endothelial cells. *PLoS One* **9**, e115981,

670   doi:10.1371/journal.pone.0115981 (2014).

671 22 Vanlandewijck, M. *et al.* A molecular atlas of cell types and zonation in the brain

672   vasculature. *Nature* **554**, 475-480, doi:10.1038/nature25739 (2018).

673 23 Liu, Q. *et al.* Lung regeneration by multipotent stem cells residing at the

27

674   bronchioalveolar-duct junction. *Nat Genet* **51**, 728-738, doi:10.1038/s41588-019-

675   0346-6 (2019).

676 24 Tang, M. *et al.* Simultaneous quantitative assessment of two distinct cell lineages

677   with a nuclear-localized dual genetic reporter. *J Mol Cell Cardiol* **146**, 60-68,

678   doi:10.1016/j.yjmcc.2020.07.002 (2020).

679 25 Picelli, S. *et al.* Full-length RNA-seq from single cells using Smart-seq2. *Nat*

680   *Protoc* **9**, 171-181, doi:10.1038/nprot.2014.006 (2014).

681 26 Kharchenko, P. V., Silberstein, L. & Scadden, D. T. Bayesian approach to single-

682   cell   differential   expression   analysis.   *Nat   Methods*   **11**,   740-742,

683   doi:10.1038/nmeth.2967 (2014).

684 27 Saadoun, S., Papadopoulos, M. C., Hara-Chikuma, M. & Verkman, A. S.

685   Impairment of angiogenesis and cell migration by targeted aquaporin-1 gene

686   disruption. *Nature* **434**, 786-792, doi:10.1038/nature03460 (2005).

687 28 Aibar, S. *et al.* SCENIC: single-cell regulatory network inference and clustering.

688   *Nat Methods* **14**, 1083-1086, doi:10.1038/nmeth.4463 (2017).

689 29 Eelen, G. *et al.* Role of glutamine synthetase in angiogenesis beyond glutamine

690   synthesis. *Nature* **561**, 63-69, doi:10.1038/s41586-018-0466-7 (2018).

691 30 Zhang, M. *et al.* CXCL12 enhances angiogenesis through CXCR7 activation in

692   human umbilical vein endothelial cells. *Sci Rep* **7**, 8289, doi:10.1038/s41598-017-

693   08840-y (2017).

694 31 Goveia, J. *et al.* An Integrated Gene Expression Landscape Profiling Approach to

695   Identify Lung Tumor Endothelial Cell Heterogeneity and Angiogenic Candidates.

696   *Cancer cell* **37**, 21-36 e13, doi:10.1016/j.ccell.2019.12.001 (2020).

697 32 Rohlenova, K. *et al.* Single-Cell RNA Sequencing Maps Endothelial Metabolic

698   Plasticity   in   Pathological   Angiogenesis.   *Cell   Metab*   **31**,   862-877   e814,

699   doi:10.1016/j.cmet.2020.03.009 (2020).

700   33   Yang, Y. & Oliver, G. Development of the mammalian lymphatic vasculature.

701   *The Journal of clinical investigation* **124**, 888-897, doi:10.1172/JCI71609 (2014).

702   34   Fujimoto, N. *et al.* Single-cell mapping reveals new markers and functions of

703   lymphatic endothelial cells in lymph nodes. *PLoS biology* **18**, e3000704,

704   doi:10.1371/journal.pbio.3000704 (2020).

705   35   Bazigou, E. *et al.* Integrin-alpha9 is required for fibronectin matrix assembly

706   during lymphatic valve morphogenesis. *Developmental cell* **17**, 175-186,

707   doi:10.1016/j.devcel.2009.06.017 (2009).

708   36   Trapnell, C. *et al.* The dynamics and regulators of cell fate decisions are revealed

709   by pseudotemporal ordering of single cells. *Nature biotechnology* **32**, 381-386,

710   doi:10.1038/nbt.2859 (2014).

711   37   Gulati, G. S. *et al.* Single-cell transcriptional diversity is a hallmark of

712   developmental potential. *Science* **367**, 405-411, doi:10.1126/science.aax0249

713   (2020).

714   38   Tushinski, R. J. *et al.* Survival of mononuclear phagocytes depends on a lineage-

715   specific growth factor that the differentiated cells selectively destroy. *Cell* **28**, 71-

716   81, doi:10.1016/0092-8674(82)90376-2 (1982).

717   39   Dai, X. M. *et al.* Targeted disruption of the mouse colony-stimulating factor 1

718   receptor gene results in osteopetrosis, mononuclear phagocyte deficiency,

719   increased primitive progenitor cell frequencies, and reproductive defects. *Blood*

720   **99**, 111-120, doi:10.1182/blood.v99.1.111 (2002).

721   40   Klotz, L. *et al.* Cardiac lymphatics are heterogeneous in origin and respond to

722   injury. *Nature* **522**, 62-67, doi:10.1038/nature14483 (2015).

723   41   Plein, A., Fantin, A., Denti, L., Pollard, J. W. & Ruhrberg, C. Erythro-myeloid

29

724   progenitors contribute endothelial cells to blood vessels. *Nature* **562**, 223-228,

725   doi:10.1038/s41586-018-0552-x (2018).

726 42 Hirschi, K. K., Ingram, D. A. & Yoder, M. C. Assessing identity, phenotype, and

727   fate of endothelial progenitor cells. *Arterioscler Thromb Vasc Biol* **28**, 1584-1595,

728   doi:10.1161/ATVBAHA.107.155960 (2008).

729 43 Mantovani, A., Marchesi, F., Malesci, A., Laghi, L. & Allavena, P. Tumour-

730   associated macrophages as treatment targets in oncology. *Nat Rev Clin Oncol* **14**,

731   399-416, doi:10.1038/nrclinonc.2016.217 (2017).

732 44 Heng, J. S. *et al.* Hypoxia tolerance in the Norrin-deficient retina and the

733   chronically hypoxic brain studied at single-cell resolution. *Proceedings of the*

734   *National Academy of Sciences of the United States of America* **116**, 9103-9114,

735   doi:10.1073/pnas.1821122116 (2019).

736 45 Folkman, J. Tumor angiogenesis: therapeutic implications. *N Engl J Med* **285**,

737   1182-1186 (1971).

738 46 Ferrara, N. & Kerbel, R. S. Angiogenesis as a therapeutic target. *Nature* **438**, 967-

739   974, doi:10.1038/nature04483 (2005).

740 47 Welti, J., Loges, S., Dimmeler, S. & Carmeliet, P. Recent molecular discoveries

741   in angiogenesis and antiangiogenic therapies in cancer. *J Clin Invest* **123**, 3190-

742   3200, doi:10.1172/JCI70212 (2013).

743 48 Zhao, Q. *et al.* Single-Cell Transcriptome Analyses Reveal Endothelial Cell

744   Heterogeneity in Tumors and Changes following Antiangiogenic Treatment.

745   *Cancer Res* **78**, 2370-2382, doi:10.1158/0008-5472.CAN-17-2728 (2018).

746 49 Bazigou, E. *et al.* Genes regulating lymphangiogenesis control venous valve

747   formation and maintenance in mice. *The Journal of clinical investigation* **121**,

748   2984-2992, doi:10.1172/JCI58050 (2011).

749 50 Subach, O. M. *et al.* Conversion of red fluorescent protein into a bright blue probe.

750   *Chem Biol* **15**, 1116-1124, doi:10.1016/j.chembiol.2008.08.006 (2008).

751 51 Tirosh, I. *et al.* Dissecting the multicellular ecosystem of metastatic melanoma by

752   single-cell RNA-seq. *Science* **352**, 189-196, doi:10.1126/science.aad0501 (2016).

753 52 Stuart, T. *et al.* Comprehensive Integration of Single-Cell Data. *Cell* **177**, 1888-

754   1902 e1821, doi:10.1016/j.cell.2019.05.031 (2019).

755 53 Lambrechts, D. *et al.* Phenotype molding of stromal cells in the lung tumor

756   microenvironment. *Nat Med* **24**, 1277-1289, doi:10.1038/s41591-018-0096-5

757   (2018).

758 54 Peng, J. *et al.* Single-cell RNA-seq highlights intra-tumoral heterogeneity and

759   malignant progression in pancreatic ductal adenocarcinoma. *Cell Res* **29**, 725-738,

760   doi:10.1038/s41422-019-0195-y (2019).

761 55 Ma, L. *et al.* Tumor Cell Biodiversity Drives Microenvironmental

762   Reprogramming in Liver Cancer. *Cancer Cell* **36**, 418-430 e416,

763   doi:10.1016/j.ccell.2019.08.007 (2019).

764 56 Yost, K. E. *et al.* Clonal replacement of tumor-specific T cells following PD-1

765   blockade. *Nat Med* **25**, 1251-1259, doi:10.1038/s41591-019-0522-3 (2019).

766 57 Cortez-Retamozo, V. *et al.* Origins of tumor-associated macrophages and

767   neutrophils. *Proc Natl Acad Sci U S A* **109**, 2491-2496,

768   doi:10.1073/pnas.1113744109 (2012).

769 58 Berg, S. *et al.* ilastik: interactive machine learning for (bio)image analysis. *Nat*

770   *Methods* **16**, 1226-1232, doi:10.1038/s41592-019-0582-9 (2019).

771 59 Wang, A., Yan, X. & Wei, Z. ImagePy: an open-source, Python-based and

772   platform-independent software package for bioimage analysis. *Bioinformatics* **34**,

773   3238-3240, doi:10.1093/bioinformatics/bty313 (2018).

774

FIGURE LEGENDS

Fig. 1: Csf1r lineage endothelial cells (CLECs) contribute to perfused, dynamically sprouting and remodeling blood vessels in mouse glioma. a, Csf1r-Mer2.CremTmG: a mouse model for Csf1r-lineage tracing combining the tamoxifen-inducible Cre-driver under control of the Csf1r-promoter and the mTmG Cre-reporter. b, Timing schedule of glioma implantation, tamoxifen induction and in vivo imaging. c-f, Longitudinal intravital imaging of the tumour vasculature in CT2A mouse glioma of Csf1r-Mer2.CremTmG by cranial window. Scale bar: 50 μm. c, In vivo imaging in 3 weeks glioma. Endothelial cells in red (tdTomato), Csf1r-labeled cells in green (GFP) and glioma cells in blue (BFP). d, Detail image of outlined square in Fig. 1c illustrating tracing of GFP-positive cells. White arrowheads, macrophages; blue arrowhead, CLECs at tip position. e, In vivo imaging of CLECs in 2 weeks glioma. Blue arrowheads, tip of endothelial cells. f, Visualization of blood vessels in 3 weeks glioma by Intravenous injection of dextran with texas red dye. Yellow arrowhead, bridging CLECs; orange arrowhead, tube formation by CLECs; blue arrowhead, CLECs at tip position. g-h, Counterstaining on PFA-fixed 4 weeks CT2A glioma sections of Csf1r-Mer2.CremTmG with indicated antibodies. Yellow arrows, CLECs. Scale bar: 25 μm.

Fig. 2: Up to 10% of intra-tumour endothelium is comprised of CLECs not only in glioma, but also in other tumour types and locations. a-i, Quantification of the population of CLECs in glioma of Csf1r-Mer2.CremTmG mice. a, Gross appearance of sham control and 4 weeks CT2A glioma (Upper panel). Purple arrowhead, the area of capillary injection; blue arrowhead, glioma. Scale bar: 5 mm. Flow cytometric analysis of CLECs in sham control and 4 weeks CT2A glioma (Lower panel). b, In 3 weeks CT2A

798   glioma (n= 9), CLECs constitute 2.1 ± 1.0% of total endothelial cells (CD45-CD31+); in

799   4 weeks CT2A glioma (n= 5), they make up 7.5 ± 1.6% of total endothelial cells. c, In 3

800   weeks GL261 glioma (n= 5), CLECs constitute 1.5 ± 1.6% of total endothelial cells. d,

801   Gross appearance of normal brain, sham control and 3 weeks CT2A glioma. Purple

802   arrowhead, area of capillary injection. Scale bar: 5 mm. e-f, Quantification of the

803   population of CLECs by flow cytometric analysis in brain and tumour samples. Bars

804   represent mean ± s.d. *p<0.05, **p<0.01, ***p<0.001, ****P<0.0001. Two-tailed

805   unpaired Mann-Whitney' s U test. i-j, Analysis of CLECs in B16F1 melanoma in Csf1r-

806   Mer2.CremTmG mice. g, Counterstaining on PFA-fixed section of day12 melanoma with

807   CDH5 antibody. Yellow arrows, CLECs. Scale bar: 50 μm. h, CLECs constitute 2.8 ±

808   0.75% of total endothelial cells in day 12 melanoma (n=4).

809   **Fig. 3: CLECs do not originate from the bone marrow.** a-b, Tamoxifen induction

810   timing. b, Quantification of the population of tumour macrophagens (T_MACs:

811   CD45+GFP+) and tumour CLECs (T_CLECs: CD45-CD31+GFP+) by flow cytometric

812   analysis in tumour samples (n=4). Bars represent mean ± s.d. c, Fluorescent images of

813   PFA-fixed 3 weeks CT2A glioma de of Csf1r-Mer2.CremTmG mice within 24 hours after

814   tamoxifen induction. Scale bar: 100 μm. d-e, Flow cytometric analysis of CT2A-glioma

815   in bone marrow chimeras. d, BMCsf1r-mer2.CremTmG: C57BL/6J mice are used as

816   recipients and Csf1r-Mer2.CremTmG mice used as donors. Within the sorted myeloid

817   cell population (BFP-CD45+), 32.3 ± 12.1% are GFP-positive in Csf1r-Mer2.CremTmG

818   mice (n= 10), and 33.8 ± 6.9% are GFP-positive in bone-marrow transplanted BMCsf1r-

819   Mer2.CremTmG mice (n= 12). Among endothelial cell population (BFP-CD45-CD31+),

820   4.3 ± 1.9% are GFP-positive in Csf1r-Mer2.CremTmG mice (n= 10), whereas no GFP-

821   positive endothelial cells are found in BMCsf1r-Mer2.CremTmG mice (n= 12). e, Csf1r-

822 Mer2.CremTmG:: BMWT: Csf1r-Mer2.CremTmG are used as recipients and C57BL/6J

823 as donors. Of the sorted myeloid cell population, $43.4 \pm 11.3\%$ GFP-positive cells are

824 found in Csf1r-Mer2.CremTmG mice (n= 6), whereas $0.1 \pm 0.1\%$ GFP-positive cells are

825 found in Csf1r-Mer2.CremTmG:: BMWT mice (n= 4). Of the endothelial cell population,

826 $10.5 \pm 9.7\%$ GFP-positive cells are found in Csf1r-Mer2.CremTmG mice (n= 6), and 9.3

827 $\pm 3.7\%$ GFP-positive cells are found in Csf1r-Mer2.CremTmG:: BMWT mice (n= 4).

828 Bars represent mean $\pm$ s.d. *$p<0.05$, **$p<0.01$, ***$p<0.001$, ****$p<0.0001$. Two-tailed

829 unpaired Mann-Whitney' s U test. e, Longitudinal intravial imaging of 2 weeks CT2A

830 glioma of Csf1r-Mer2.CremTmG and Csf1r-Mer2.CremTmG :: BMWT mice. White

831 arrows, CLECs. Scale bar: 50 μm.

832 **Fig. 4: Dual recombination lineage tracing and inducible depletion model identifies**

833 **a role for CLECs in tumour blood vessel patterning supporting glioma growth.** a,

834 Cdh5-Dre: Csf1r-Mer2.Cre: RSR-LSL-tdTomato (DreMer2.CretdTomato): a genetic

835 mouse model for CLEC selective tracing by dual recombination. b-c, Analysis in

836 DreMer2.CretdTomato. b, Longitudinal intravital imaging of the tumour vasculature in 3

837 weeks CT2A mouse glioma by Intravenous injection of FITC dextran. Yellow

838 arrowheads, CLECs. Scale bar: 50 μm. c, ERG antibody counterstaining on PFA-fixed

839 sections of 3 weeks CT2A glioma. Yellow arrows, CLECs. Scale bar: 50 μm. d, Cdh5-

840 Dre: Csf1r-Mer2.Cre: RSR-mTmG-DTR (DreMer2.CremTmG-DTR): a genetic mouse

841 model for CLEC selective tracing and inducible ablation. DTR, diphtheria toxin receptor.

842 e-m, Analysis in DreMer2.CremTmG-DTR. e, Longitudinal intravital imaging of the

843 tumour vasculature in 3 weeks CT2A mouse glioma. Mer2.CremTmG, Csf1r-

844 Mer2.CremTmG. Yellow arrowheads, CLECs. f, Timing schedule of glioma implantation,

845 tamoxifen induction and diphtheria toxin (DT) treatment. g, Gross appearance of 3 weeks

34

846   CT2A gliomas. Scale bar: 5 mm. h, Confocal images of PFA-fixed 3 weeks CT2A glioma

847   sections. Yellow arrows, CLECs. Scale bar: 50 μm. i, Tumour weight at 3 weeks CT2A

848   glioma. j-l, Analysis of PFA-fixed 3 weeks CT2A glioma sections. j, Tumour blood

849   vessels area. k, Network length of tumour blood vessels. l, Number of bifurcations of

850   tumour blood vessels. Bars represent mean ± s.d. *p<0.05, **p<0.01. Two-tailed unpaired

851   Mann-Whitney's U test.

852   **Fig. 5: Single-cell analysis identifies a unique signature that defines the tumour**

853   **CLECs.** a-d, Single-cell RNA sequencing (scRNA-seq) analysis of tumour macrophages

854   (T_MACs: CD45+GFP+, 79 cells), tumour endothelial cell (T_ECs: CD45-CD31+GFP-,

855   78 cells), tumour CLECs (T_CLECs: CD45-CD31+GFP+, 141 cells) in 4 weeks CT2A

856   glioma of Csf1r-Mer2.CremTmG mice. b, Gene expression of typical endothelial cell

857   markers, macrophages and myeloid cell markers. c, Csf1r gene expression. d, Three

858   characteristic genes expressed in T_CLECs. e, Enrichment of Tip-cell signature in

859   T_CLECs compared to T_ECs as shown by GSEA. f-k, Analysis of scRNA-seq data of

860   human endothelial cells from multiple primary tumours. f, UMAP plot of human

861   endothelial cell subtypes. g, UMAP plot of human endothelial cells colour-coded for the

862   tumour type of origins. h, UMAP plots with marker gene expression for each EC subtype.

863   i, Heatmap of marker gene expression for each EC phenotype (each cell as a column and

864   each gene as a row). j-k, AUCell analysis of 24 T_CLECs markers. j, T_CLECs

865   subpopulation indicated (AUC>0.165) by red colored dots. k, Cell type-specific (left) and

866   tumour type-specific (right) populations of T_CLECs. BCC, basal cell carninoma: PDAC,

867   pancreatic ductal adenocarcinoma.

868   **Fig. 6: CLECs are linked to Prox1-positive lymphatic endothelium of the**

869   **subcapsular sinus floor in lymph nodes.** a, Fluorescent images of the indicated organs

870 of Csf1r-Mer2.CremTmG mice after multiple tamoxifen induction. Scale bar: 50 µm. b,

871 Quantification of the population of CLECs in Csf1r-Mer2.CremTmG mice by flow

872 cytmetric analysis. Of the endothelial cell population (CD45-CD31+), 9.8 ± 2.1% GFP-

873 positive cells are found in the axillary lymph node of Csf1r-Mer2.CremTmG mice (n=

874 10). c, Counterstaining on PFA-fixed Inguinal lymph node of Csf1r-Mer2.CremTmG::

875 BMWT mice using PROX1 antibody within 24 hours after tamoxifen induction. Yellow

876 arrowheads, GFP+tdTomato+PROX1+ cells in the floor of the subcapsular sinus. Scale

877 bar 25 µm. d, Fluorescent images of PROX1 antibody counterstaining on PFA-fixed

878 inguinal lymph node of Csf1r-Mer2.CremTmG::BMWT mice after multiple rounds of

879 tamoxifen induction. Scale bar: 100 µm. Detailed image of square outlined in d. Yellow

880 arrowheads, GFP+Prox1+ cells; blue arrowheads, GFP+Prox1- cells. h-k, Analysis of

881 CT2A glioma in Prox1-CreERT2mTmG mice.

882 **Fig. 7: CLEC and EC heterogeneity in tumor and lymph node.** a, Quality measures

883 of 4 SMARTseq2 scRNA-seq. libraries: Csf1r-lineage endothelial cells (CLECs) and

884 endothelial cells (ECs) isolated from tumor (T_) and lymph node (LN_). b, Violin plots

885 show GFP expression per single cell. c, Uniform manifold approximation and projection

886 (UMAP) of T_CLECs, T_ECs and LN_CLECs, LN_ECs. d, Heatmap shows the 20 most

887 characteristic markers per cell population. e, UMAP colored by gene expression diversity

888 (CytoTRACE score) and predicted ordering by CytoTRACE. f, Monocle based trajectory

889 analysis of four cell populations, colored by pseudotime and CytoTRACE score.

890 **Extended Data Fig. 1: CLECs in mouse glioma express endothelial cell markers, but**

891 **lack macrophage and myeloid cell markers.** Counterstaining on PFA-fixed 4 weeks

892 CT2A glioma sections of Csf1r-Mer2.CremTmG with indicated antibodies. Lower panels

893 show the detail images of outlined squares in upper panels. Yellow arrowheads, CLECs;

894 blue arrowheads, macrophages. Scale bar: 25 μm.

895 **Extended Data Fig. 2: CLECs contribute to lymphatic endothelium in the tumour**

896 **environment.** Fluorescent images of counterstaining on PFA-fixed section of day 12

897 B16F1 melanoma under ear skin of Csf1r-Mer2.CremTmG mice using LYVE1 antibody.

898 Lower panel indicates detail image of yellow outlined square in upper panel. Yellow

899 arrow heads, CLECs. Scale bar: 100 μm.

900 **Extended Data Fig. 3: Reconstitution rate in bone marrow chimeras**. Reconstitution

901 rate was determined in peripheral blood 8 weeks after bone marrow transplantation.

902 TdTomato-positive cells in blood of: C57BL/6J (0.3 ± 0.1%, n= 6), Csf1r-

903 Mer2.CremTmG (99.2 ± 0.5%, n= 7), BMCsf1r-Mer2.CremTmG (97.3 ± 1.6%, n= 13).

904 Bars represent mean ± s.d. ****$p<0.0001$. Two-tailed unpaired Mann-Whitney' s U test.

905 **Extended Data Fig. 4: CLECs do not originate from spleen.** Surgical removal of

906 spleen (splenectomy) was performed 3 weeks before glioma injection. CLECs isolated

907 from CT2A glioma of sham control Csf1r-Mer2.CremTmG mice (n= 5) constitute 1.5 ±

908 0.8 % of total tumour endothelial cell population, compared to 1.5 ± 0.5% found in Csf1r-

909 Mer2.CremTmG with splenectomy (n= 4). Bars represent mean ± s.d. Two-tailed

910 unpaired Mann-Whitney' s U test.

911 **Extended Data Fig. 5: CLECs locate at peripheral area of mouse glioma**. a,

912 Vibratome section (200 μm-thick) of 4 weeks CT2A glioma of Csf1r-Mer2.CremTmG::

913 BMWT mice. Scale bar: 1 mm. b, Fluorescent images of area outlined in a. Yellow

914 arrowheads, CLECs. Scale bar: 100 μm.

915 **Extended Data Fig. 6: 24 tumour CLECs markers in mouse glioma.** SCDE analysis

916 of scRNA-seq data of tumour macrophages (T_MACs: CD45+GFP+, n= 79), tumour

917 endothelial cells (T_ECs: CD45-CD31+GFP-, n= 78), tumour CLECs (T_CLECs: CD45-

918 CD31+GFP+, n= 141) in 4 weeks CT2A glioma in Csf1r-Mer2.CremTmG mice. Bars

919 represent mean ± s.d. $*p<0.05$, $**p<0.01$, $***p<0.001$, $****p<0.0001$. Two-tailed

920 unpaired t-test with Welch correction.

921 **Extended Data Fig. 7: CLECs in glioma express AQP1**. Counterstaining on PFA-fixed

922 CT2A glioma of Csf1r-Mer2.CremTmG::BMWT mice using AQP1 antibody. Yellow

923 arrowheads, T_CLECs; blue arrowheads, T_ECs. Scale bar: 25 μm.

924 **Extended Data Fig. 8: CLECs in glioma cannot be labelled by GFP within 24 hours**

925 **after tamoxifen induction.** a-b, Tamoxifen induction timing. b, Quantification of the

926 population of tumour macrophagens (T_MACs: CD45+GFP+) and tumour CLECs

927 (T_CLECs: CD45-CD31+GFP+) by flow cytometric analysis in tumour samples (n=4).

928 Bars represent mean ± s.d. c, Fluorescent images of PFA-fixed 3 weeks CT2A glioma de

929 of Csf1r-Mer2.CremTmG mice within 24 hours after tamoxifen induction. Scale bar: 100

930 μm.

931 **Extended Data Fig. 9: CLEC and EC heterogeneity in tumor and lymph node** .

932 a, Heatmap shows the expression of n=91 fLECs markers in LN_CLEC, LN_EC,

933 T_CLEC and T_EC single cells. b, Violin plots show the expression of 3 CLEC markers:

934 Pde4d, Robo1 and Itga9.

935 **Supplemental Movie 1: Time-lapse *in vivo* imaging of Csf1r lineage endothelial tip**

936 **cell in CT2A glioma of *Csf1r-Mer2.Cre^{mTmG}* mice.** Imaging was performed over 4 hours

937 (1 frame/ 10 min).

938

939   **Supplemental Movie 2: Time-lapse *in vivo* imaging of *Csf1r* lineage endothelial tip**

940   **cell in CT2A glioma of *Csf1r-Mer2.Cre^{mTmG}*::BM^{WT}.** Imaging was performed over 50

941   minutes (1 frame/ 2.5 min).

942

943   **Supplemental Table 1:   Details of gene expression analysis.** Seurat based differential

944   analysis (non-parameteric Wilcoxon rank sum test) was performed by comparing cell

945   types amongst each other (green columns) and the different Seurat clusters (yellow

946   columns). p_val: p_val (unadjusted). avg_logFC: log fold-change of the average

947   expression between the two groups. Positive values indicate that the feature is more

948   highly expressed in the first group. pct.1: The percentage of cells where the feature is

949   detected in the first group. pct.2: The percentage of cells where the feature is detected in

950   the second group. p_val_adj: Adjusted p-value, based on Bonferroni correction using all

951   features in the dataset.

952

953   **Supplemental Table 2:   Marker genes for EC subtypes of multiple tumour types.**

954   p_val: p_val (unadjusted). avg_logFC: Average log (fold change). pct.1: Percentage of

955   expressed cells in current cluster. pct.2: Percentage of expressed cells in other cluster.

956   p_val_adj: Adjusted p-value. cluster: Cluster name. gene: Gene name. log2fc: log2 (fold

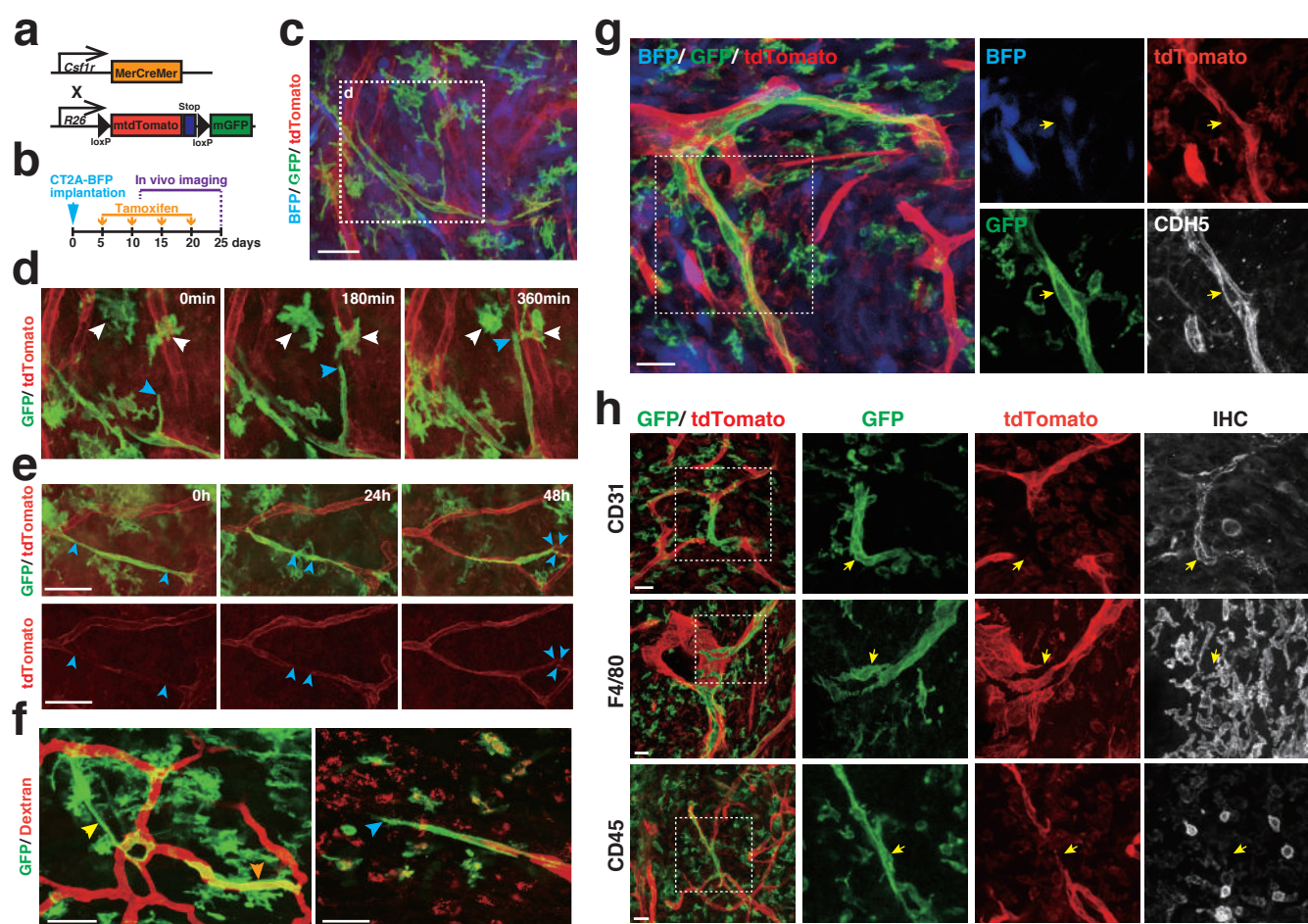957   change). Log2pct: log2 ((pct+0.005)/(pct2+0.005)).

958

Fig. 1: *Csf1r* **lineage endothelial cells (CLECs) contribute to perfused, dynamically sprouting and remodeling blood vessels in mouse glioma.** a, *Csf1r-Mer2.Cre*^{mTmG}: a mouse model for *Csf1r*-lineage tracing combining the tamoxifen-inducible Cre-driver under control of the *Csf1r*-promoter and the *mTmG* Cre-reporter. b, Timing schedule of glioma implantation, tamoxifen induction and in vivo imaging. c-f, Longitudinal intravital imaging of the tumour vasculature in CT2A mouse glioma of *Csf1r-Mer2.Cre*^{mTmG} by cranial window. Scale bar: 50 μm. c, In vivo imaging in 3 weeks glioma. Endothelial cells in red (tdTomato), *Csf1r*-labeled cells in green (GFP) and glioma cells in blue (BFP). d, Detail image of outlined square in Fig. 1c illustrating tracing of GFP-positive cells. White arrowheads, macrophages; blue arrowhead, CLECs at tip position. e, In vivo imaging of CLECs in 2 weeks glioma. Blue arrowheads, tip of endothelial cells. f, Visualization of blood vessels in 3 weeks glioma by Intravenous injection of dextran with texas red dye. Yellow arrowhead, bridging CLECs; orange arrowhead, tube formation by CLECs; blue arrowhead, CLECs at tip position. g-h, Counterstaining on PFA-fixed 4 weeks CT2A glioma sections of *Csf1r-Mer2.Cre*^{mTmG} with indicated antibodies. Yellow arrows, CLECs. Scale bar: 25 μm.
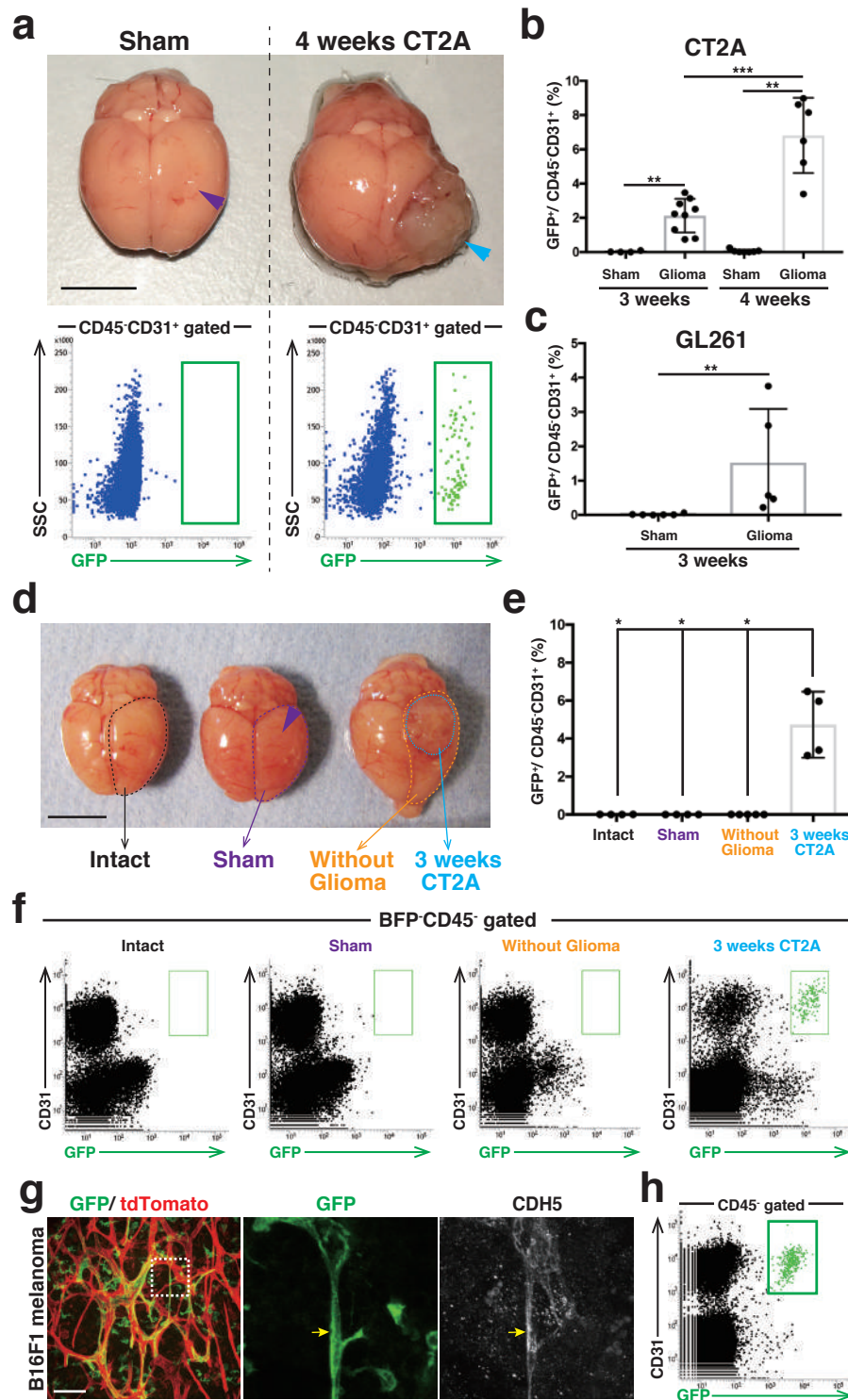
Matsumoto K et al., Figure1

Fig. 2: Up to 10% of intra-tumour endothelium is comprised of CLECs not only in glioma, but also in other tumour types and locations. a-f, Quantification of the population of CLECs in glioma of Csf1r-Mer2.Cre^mTmG mice. a, Gross appearance of sham control and 4 weeks CT2A glioma (Upper panel). Purple arrowhead, the area of capillary injection; blue arrowhead, glioma. Scale bar: 5 mm. Flow cytometric analysis of CLECs in sham control and 4 weeks CT2A glioma (Lower panel). b, In 3 weeks CT2A glioma (n= 9), CLECs constitute 2.1 ± 1.0% of total endothelial cells (CD45-CD31+); in 4 weeks CT2A glioma (n= 5), they make up 7.5 ± 1.6% of total endothelial cells. c, In 3 weeks GL261 glioma (n=5), CLECs constitute 1.5 ± 1.6% of total endothelial cells. d, Gross appearance of normal brain, sham control and 3 weeks CT2A glioma. Purple arrowhead, area of capillary injection. Scale bar: 5 mm. e-f, Quantification of the population of CLECs by flow cytometric analysis in brain and tumour samples. Bars represent mean ± s.d. *P<0.05, **P<0.01, ***P<0.001, ****P<0.0001. Two-tailed unpaired Mann-Whitney's U test. g-h, Analysis of CLECs in B16F1 melanoma in Csf1r-Mer2.CremTmG mice. g, Counterstaining on PFA-fixed section of day12 melanoma with CDH5 antibody. Yellow arrows, CLECs. Scale bar: 50 μm. h, CLECs constitute 2.8 ± 0.75% of total endothelial cells in day 12 melanoma (n=4).
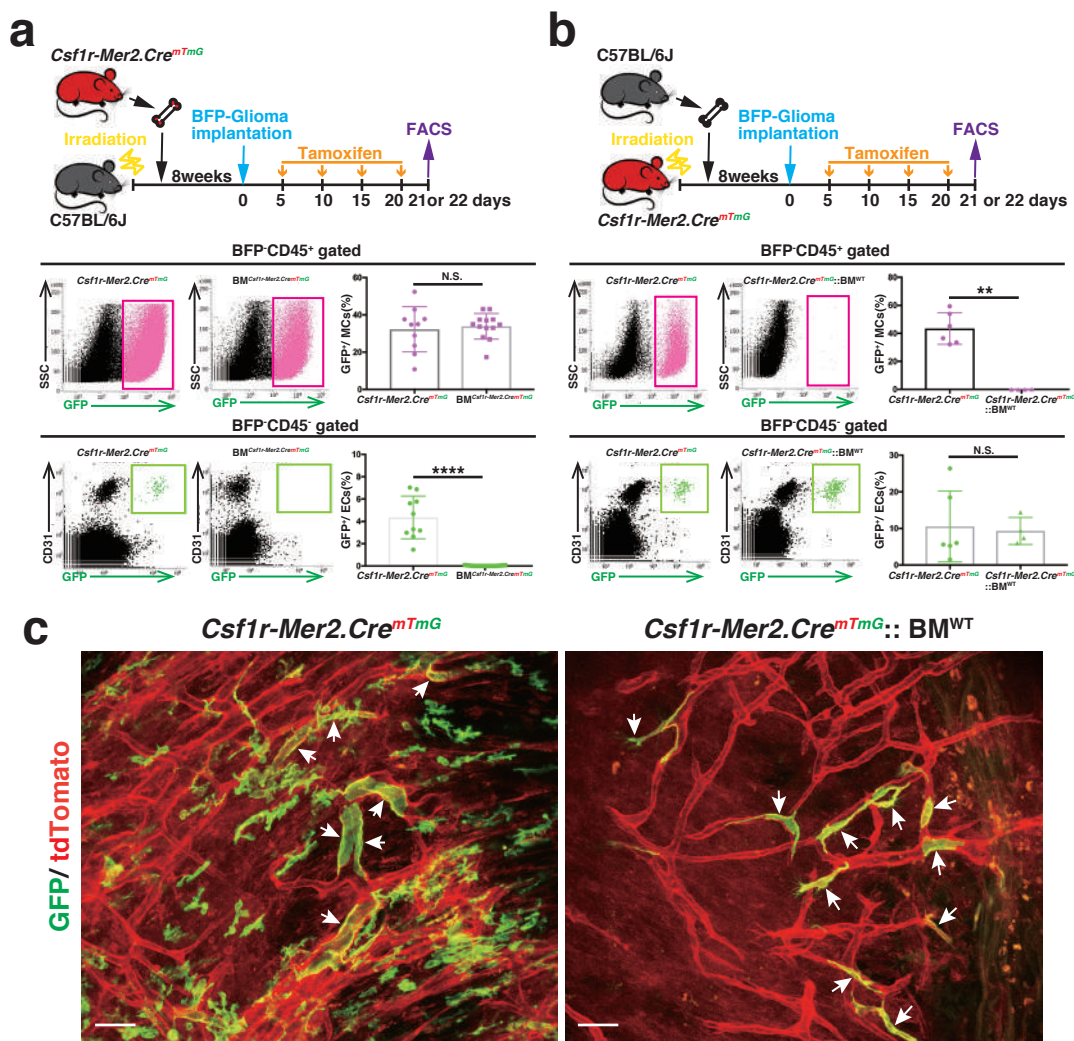
Matsumoto K et al., Figure 2

Fig. 3: CLECs do not originate from bone marrow. a-b, Flow cytometric analysis of CT2A-glioma in bone marrow chimeras.

a, BM$^{Csf1r-mer2.CremTmG}$: C57BL/6J mice are used as recipients and *Csf1r-Mer2.Cre^{mTmG}* mice used as donors. Within the sorted myeloid cell population (BFP⁻CD45⁺), 32.3 ± 12.1% are GFP-positive in *Csf1r-Mer2.Cre^{mTmG}* mice (n= 10), and 33.8 ± 6.9% are GFP-positive in bone-marrow transplanted BM$^{Csf1r-Mer2.CremTmG}$ mice (n= 12). Among endothelial cell population (BFP⁻CD45⁻CD31⁺), 4.3 ± 1.9% are GFP-positive in *Csf1r-Mer2.Cre^{mTmG}* mice (n= 10), whereas no GFP-positive endothelial cells are found in BM$^{Csf1r-Mer2.CremTmG}$ mice (n= 12). b, *Csf1r-Mer2.Cre^{mTmG}*:: BM^{WT}: *Csf1r-Mer2.Cre^{mTmG}* are used as recipients and C57BL/6J as donors. Of the sorted myeloid cell population, 43.4 ± 11.3% GFP-positive cells are found in *Csf1r-Mer2.Cre^{mTmG}* mice (n= 6), whereas 0.1 ± 0.1% GFP-positive cells are found in *Csf1r-Mer2.Cre^{mTmG}*:: BM^{WT} mice (n= 4). Of the endothelial cell population, 10.5 ± 9.7% GFP-positive cells are found in *Csf1r-Mer2.Cre^{mTmG}* mice (n= 6), and 9.3 ± 3.7% GFP-positive cells are found in *Csf1r-Mer2.Cre^{mTmG}*:: BM^{WT} mice (n= 4). Bars represent mean ± s.d. *P<0.05,**P<0.01,***P<0.001, ****P<0.0001. Two-tailed unpaired Mann-Whitney' s U test. c, Longitudinal intravial imaging of 2 weeks CT2A glioma of *Csf1r-Mer2.Cre^{mTmG}* and *Csf1r-Mer2.Cre^{mTmG}* :: BM^{WT} mice. White arrows, CLECs. Scale bar: 50 *μ*m.
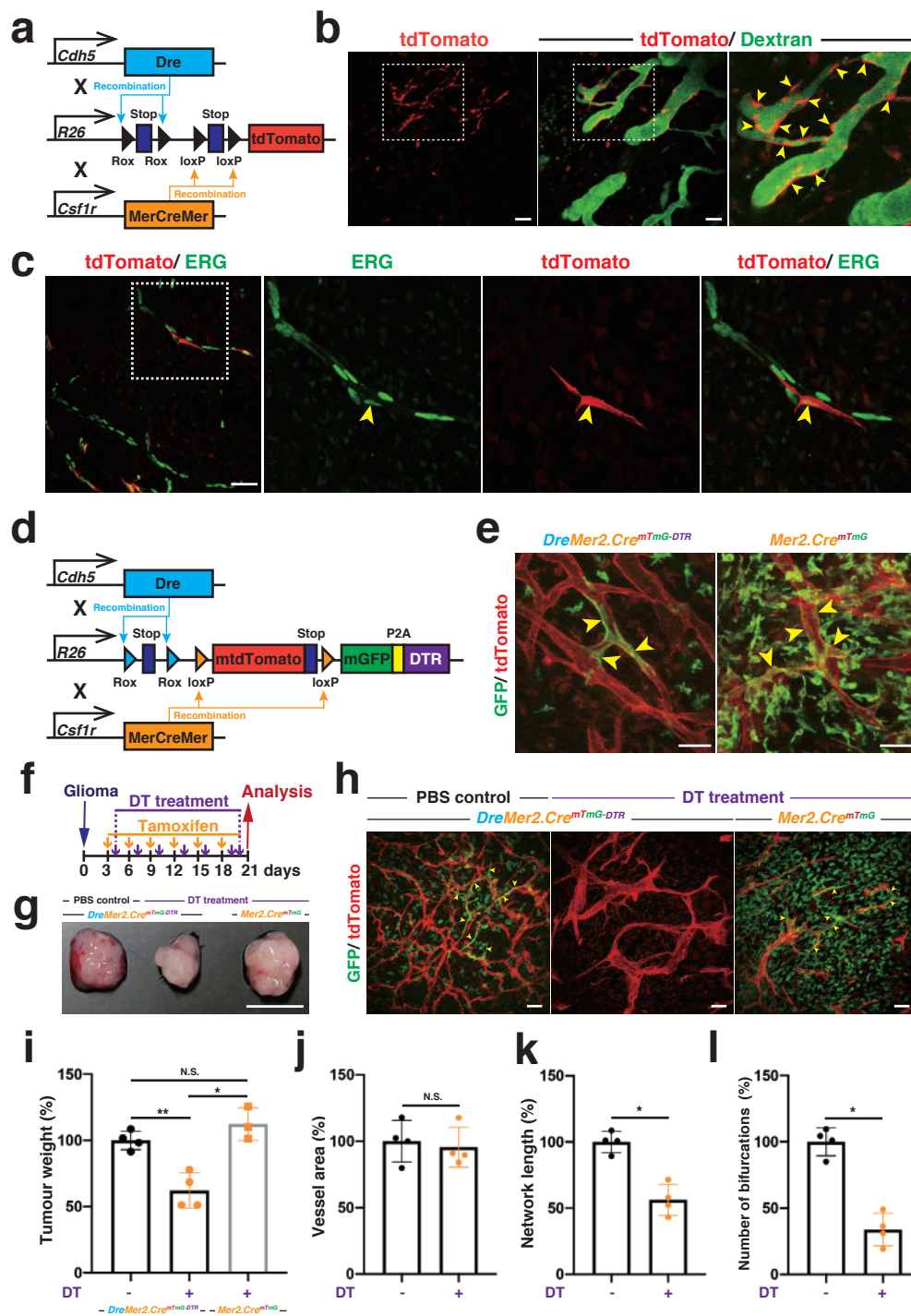
Matsumoto K et al., Figure 3

Fig. 4: Dual recombination lineage tracing and inducible depletion model identifies a role for CLECs in tumour blood vessel patterning supporting glioma growth. a, *Cdh5-Dre*: *Csf1r-Mer2.Cre*: *RSR-LSL-tdTomato* (*DreMer2.Cre^tdTomato*): a genetic mouse model for CLEC selective tracing by dual recombination. b-c, Analysis in *DreMer2.Cre^tdTomato*. b, Longitudinal intravital imaging of the tumour vasculature in 3 weeks CT2A mouse glioma by Intravenous injection of FITC dextran. Yellow arrowheads, CLECs. Scale bar: 50 μm. c, ERG antibody counterstaining on PFA-fixed sections of 3 weeks CT2A glioma. Yellow arrows, CLECs. Scale bar: 50 μm. d, *Cdh5-Dre*: *Csf1r-Mer2.Cre*: *RSR-mTmG-DTR* (*DreMer2.Cre^mTmG-DTR*): a genetic mouse model for CLEC selective tracing and inducible ablation. DTR, diphtheria toxin receptor. e-l, Analysis in *DreMer2.Cre^mTmG-DTR*. e, Longitudinal intravital imaging of the tumour vasculature in 3 weeks CT2A mouse glioma. *Mer2.Cre^mTmG*, *Csf1r-Mer2.Cre^mTmG*. Yellow arrowheads, CLECs. f, Timing schedule of glioma implantation, tamoxifen induction and diphtheria toxin (DT) treatment. g, Gross appearance of 3 weeks CT2A gliomas. Scale bar: 5 mm. h, Confocal images of PFA-fixed 3 weeks CT2A glioma sections. Yellow arrows, CLECs. Scale bar: 50 μm. i, Tumour weight at 3 weeks CT2A glioma. j-l, Analysis of PFA-fixed 3 weeks CT2A glioma sections. j, Tumour blood vessels area. k, Network length of tumour blood vessels. l, Number of bifurcations of tumour blood vessels. Bars represent mean ± s.d. *P<0.05, **P<0.01. Two-tailed unpaired Mann-Whitney's U test.
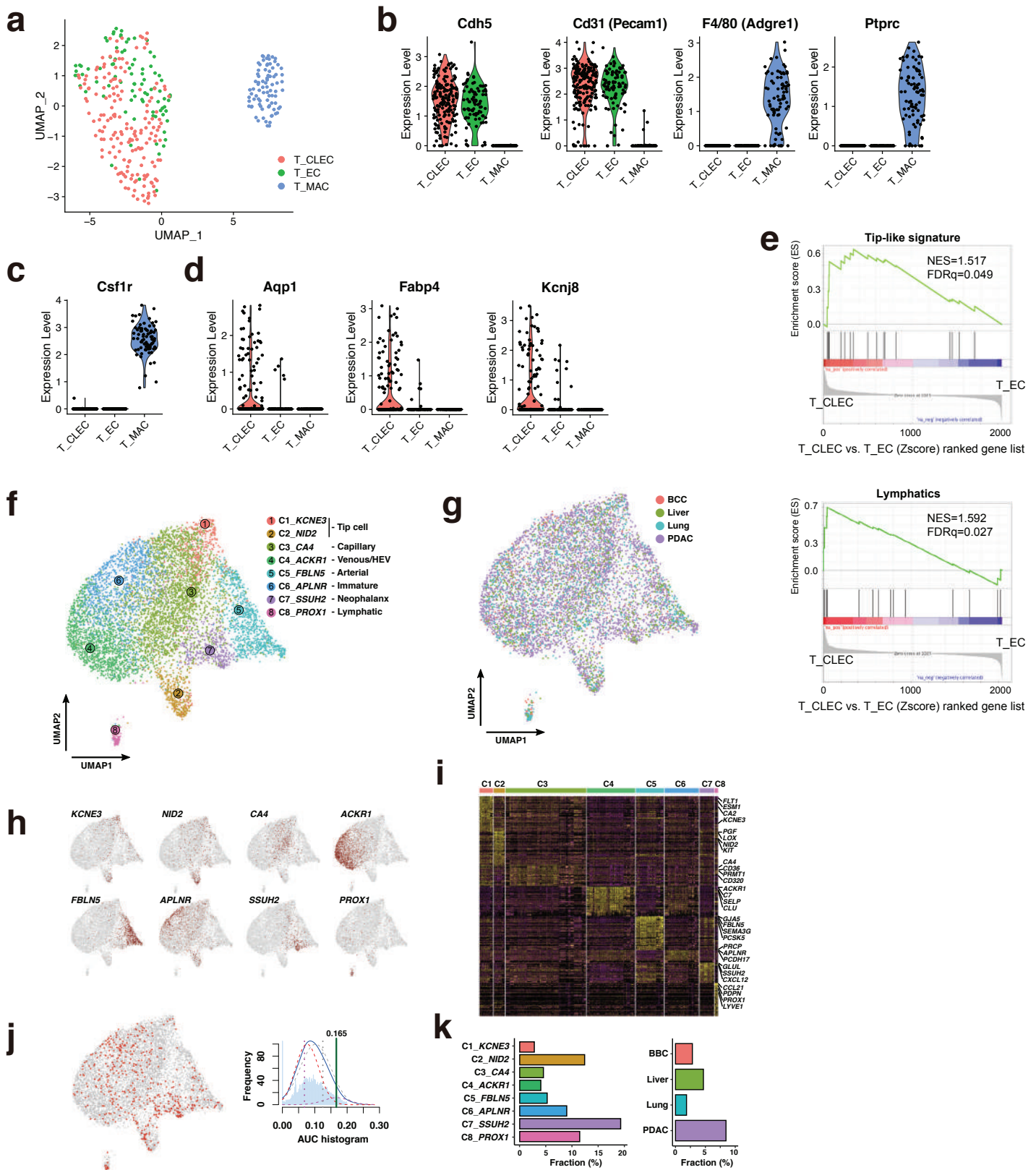
Matsumoto K et al., Figure 4

Fig. 5: Single-cell analysis identifies a unique signature that defines the tumour CLECs. a-d, Single-cell RNA sequencing (scRNA-seq) analysis of tumour macrophages (T_MACs: CD45+GFP+, 79 cells), tumour endothelial cell (T_ECs: CD45-CD31+GFP-, 78 cells), tumour CLECs (T_CLECs: CD45-CD31+GFP+, 141 cells) in 4 weeks CT2A glioma of *Csf1r-Mer2.Cre^mTmG* mice. b, Gene expression of typical endothelial cell markers, macrophages and myeloid cell markers. c, *Csf1r* gene expression. d, Three characteristic genes expressed in T_CLECs. e, Enrichment of Tip-cell and lymphatic signature in T_CLECs compared to T_ECs as shown by GSEA. f-k, Analysis of scRNA-seq data of human endothelial cells from multiple primary tumours. f, UMAP plot of human endothelial cell subtypes. g, UMAP plot of human endothelial cells colour-coded for the tumour type of origins. h, UMAP plots with marker gene expression for each EC subtype. i, Heatmap of marker gene expression for each EC phenotype (each cell as a column and each gene as a row). j-k, AUCell analysis of 24 T_CLECs markers. j, T_CLECs subpopulation indicated (AUC>0.165) by red colored dots. k, Cell type-specific (left) and tumour type-specific (right) populations of T_CLECs. BCC, basal cell carcinoma: PDAC, pancreatic ductal adenocarcinoma.
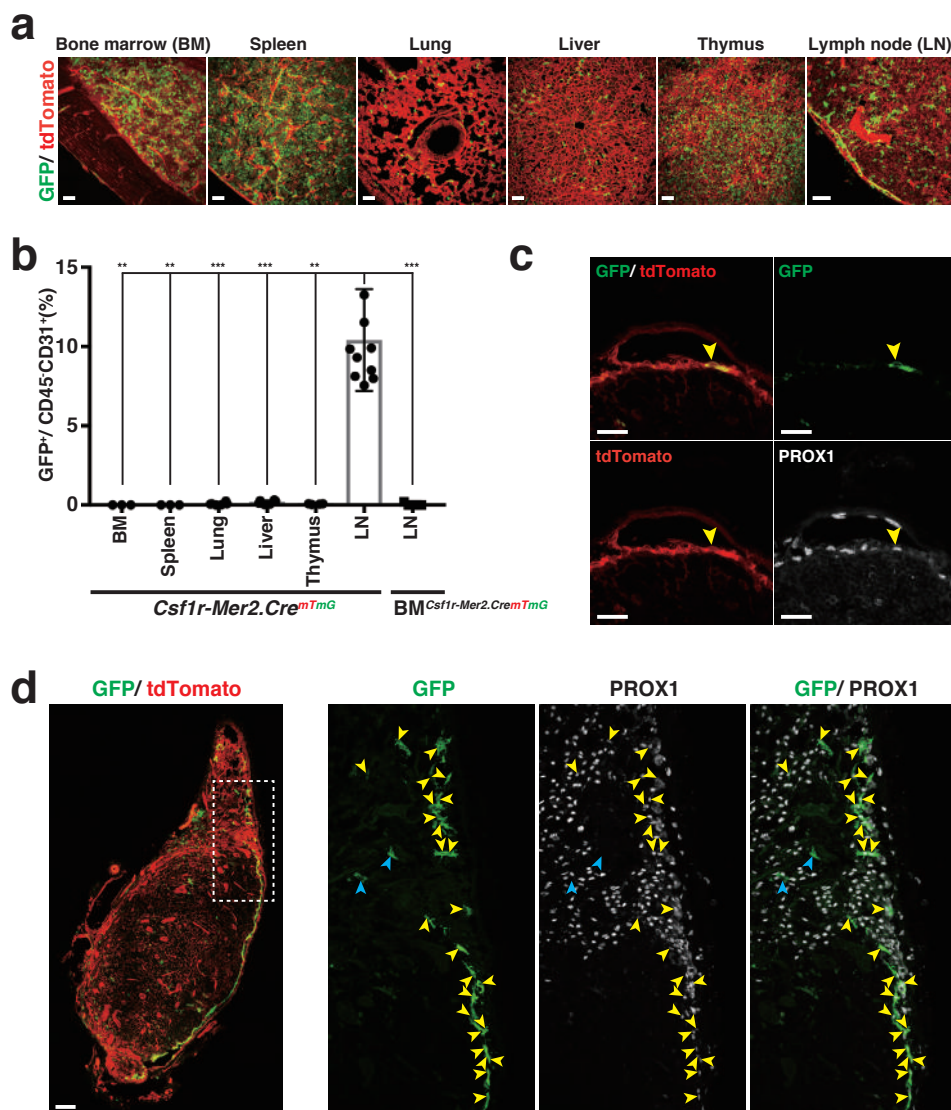
Matsumoto K et al., Figure 5

Fig. 6: CLECs are linked to *Prox1*-positive lymphatic endothelium of the subcapsular sinus floor in lymph nodes. a, Fluorescent images of the indicated organs of *Csf1r-Mer2.Cre^mTmG* mice after multiple tamoxifen induction. Scale bar: 50 μm. b, Quantification of the population of CLECs in *Csf1r-Mer2.Cre^mTmG* mice by flow cytmetric analysis. Of the endothelial cell population (CD45⁻CD31⁺), 9.8 ± 2.1% GFP-positive cells are found in the axillary lymph node of *Csf1r-Mer2.Cre^mTmG* mice (n= 10). c, Counterstaining on PFA-fixed Inguinal lymph node of *Csf1r-Mer2.Cre^mTmG*:: BM^WT mice using PROX1 antibody within 24 hours after tamoxifen induction. Yellow arrowheads, GFP⁺tdTomato⁺PROX1⁺ cells in the floor of the subcapsular sinus. Scale bar 25 μm. d, Fluorescent images of PROX1 antibody counterstaining on PFA-fixed inguinal lymph node of *Csf1r-Mer2.Cre^mTmG*::BM^WT mice after multiple rounds of tamoxifen induction. Scale bar: 100 μm. Detailed image of square outlined in d. Yellow arrowheads, GFP⁺Prox1⁺ cells; blue arrowheads, GFP⁺Prox1⁻ cells.
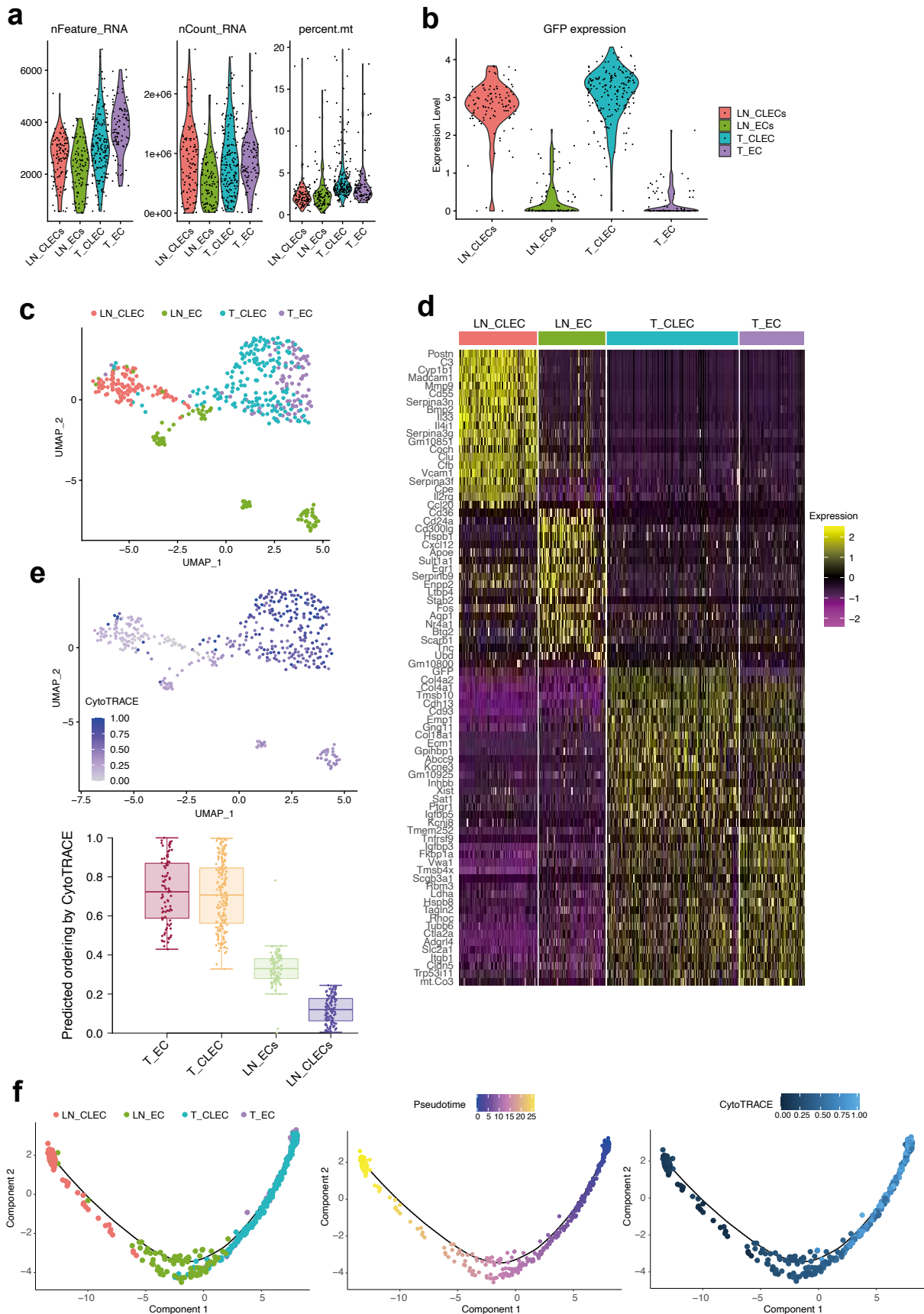
Matsumoto K et al., Figure 6

Fig. 7: CLEC and EC heterogeneity in tumor and lymph node .

a, Quality measures of 4 SMARTseq2 scRNA-seq. libraries: Csf1r-lineage endothelial cells (CLECs) and endothelial cells (ECs) isolated from tumor (T_) and lymph node (LN_). b, Violin plots show GFP expression per single cell. c, Uniform manifold approximation and projection (UMAP) of T_CLECs, T_ECs and LN_CLECs, LN_ECs. d, Heatmap shows the 20 most characteristic markers per cell population. e, UMAP colored by gene expression diversity (CytoTRACE score) and predicted ordering by CytoTRACE. f, Monocle based trajectory analysis of four cell populations, colored by pseudotime and CytoTRACE score.

Matsumoto K et al., Figure 7